Nuclear Deexcitation Gamma Ray Lines from Accelerated Particle Interactions

Benzion Kozlovsky

School of Physics and Astronomy, Tel Aviv University, Ramat Aviv, Israel

Ronald J. Murphy

E. O. Hulburt Center for Space Science, Naval Research Laboratory, Washington DC 20375

Reuven Ramaty[1]

Laboratory for High Energy Astrophysics, Goddard Space Flight Center, Greenbelt MD 20771

ABSTRACT

Total cross sections for the production of gamma-ray lines from nuclear deexcitation as a function of the projectile energy are evaluated and presented. Included are proton and α reactions with He, C, N, O, Ne, Mg, Al, Si, S, Ca and Fe. Such functions are essential for interpretation of gamma-ray line observations of astrophysical sites which contain large fluxes of energetic particles such as solar flares, the Earth's atmosphere, planetary atmospheres and surfaces, the interstellar medium and galactic nebulae.

Subject headings: Sun: abundances — Sun: flares — Sun: gamma rays — gamma rays: theory — nuclear reactions — acceleration of particles

1. Introduction

A comprehensive treatment of nuclear deexcitation gamma-ray line emission was given by Ramaty, Kozlovsky & Lingenfelter (1979) (hereafter RKL). This treatment has provided the theoretical framework for numerous investigations of gamma-ray lines observed with various space missions including the *Solar Maximum Mission*/Gamma Ray Spectrometer (Chupp 1984; Murphy et al. 1991; Share & Murphy 1995), all four *Compton Gamma Ray*

[1]Deceased

Report Documentation Page

Form Approved
OMB No. 0704-0188

1. REPORT DATE	2. REPORT TYPE	3. DATES COVERED
2002		**00-00-2002 to 00-00-2002**

4. TITLE AND SUBTITLE	5a. CONTRACT NUMBER
Nuclear Deexcitation Gamma Ray Lines from Accelerated Particle Interactions	5b. GRANT NUMBER
	5c. PROGRAM ELEMENT NUMBER
6. AUTHOR(S)	5d. PROJECT NUMBER
	5e. TASK NUMBER
	5f. WORK UNIT NUMBER
7. PERFORMING ORGANIZATION NAME(S) AND ADDRESS(ES) **Naval Research Laboratory,E. O. Hulburt Center for Space Research,4555 Overlook Avenue, SW,Washington,DC,20375**	8. PERFORMING ORGANIZATION REPORT NUMBER
9. SPONSORING/MONITORING AGENCY NAME(S) AND ADDRESS(ES)	10. SPONSOR/MONITOR'S ACRONYM(S)
	11. SPONSOR/MONITOR'S REPORT NUMBER(S)

12. DISTRIBUTION/AVAILABILITY STATEMENT
Approved for public release; distribution unlimited

13. SUPPLEMENTARY NOTES
ApJ Supp., 141, 523, (2002).

14. ABSTRACT
Total cross sections for the production of gamma-ray lines from nuclear deexcitation as a function of the projectile energy are evaluated and presented. Included are proton and α reactions with He, C, N, O, Ne, Mg, Al, Si, S, Ca and Fe. Such functions are essential for interpretation of gamma-ray line observations of astrophysical sites which contain large fluxes of energetic particles such as solar flares, the Earth?s atmosphere, planetary atmospheres and surfaces, the interstellar medium and galactic nebulae.

15. SUBJECT TERMS

16. SECURITY CLASSIFICATION OF:			17. LIMITATION OF ABSTRACT	18. NUMBER OF PAGES	19a. NAME OF RESPONSIBLE PERSON
a. REPORT	b. ABSTRACT	c. THIS PAGE			
unclassified	**unclassified**	**unclassified**	**Same as Report (SAR)**	**56**	

Observatory (*CGRO*) instruments (Share et al. 1997), Hinotori (Yoshimori 1990), Yohkoh (Yoshimori et al. 1994), GAMMA-1 (Leikov et al. 1993) and GRANAT/Phebus (Trottet et al. 1996). The results of these efforts have established gamma-ray spectroscopy as an important tool for exploration of high-energy processes in solar flares. The gamma-ray count spectrum of the 1991 June 4 solar flare obtained with the Oriented Scintillation Spectrometer Experiment (OSSE) on *CGRO* (Murphy et al. 1997) is shown in Figure 1. Among the main results of the investigations using gamma-ray spectroscopy are (1) the determination of the composition of the ambient solar atmosphere showing that the first ionization potential (FIP) effect (the enrichment of elements with low FIP known to be present in the corona and solar wind (Feldman 1992; Reames 1998; Geiss 1998)) already exists in the region where the gamma-ray production takes place (thought to be the chromosphere), placing new constraints on the origin of the effect (Murphy et al. 1991; Ramaty et al. 1995, 1996); (2) the determination of the composition of the accelerated particles interacting at the Sun revealing enhanced α/proton and ^{3}He/^{4}He ratios in many flares (Share & Murphy 1997; Mandzhavidze et al. 1999); and (3) that there are flares in which the energy contained in accelerated ions above 1 MeV is a significant fraction of that contained in accelerated electrons above 20 keV, contrary to the previously accepted paradigm that the bulk of the energy contained in accelerated particles always resides in electrons (Ramaty et al. 1995; Ramaty & Mandzhavidze 2000a).

The successful application of gamma-ray production theory in the analysis of solar flare data depends primarily on the knowledge of the various nuclear reaction cross sections. Since 1979, gamma-ray line investigations based on RKL have regularly incorporated new laboratory measurements of cross sections, new and improved theoretical evaluations of cross sections, and the addition of more gamma-ray lines in the analyses. These improvements have not been discussed in the publications associated with these investigations. The purpose of this paper is to provide a detailed description of these improvements so that the basis of the research and the results can be better understood. A thorough knowledge of the characteristics and behavior of the cross sections will be even more essential when high spectral resolution data become available (e.g, with the launch of HESSI) and many more lines, including weaker lines, will be detected and resolved.

Based on the principles delineated by RKL, a Monte Carlo computer code was developed to calculate the expected gamma-ray spectrum from nuclear deexcitation lines for any ambient and accelerated particle composition and accelerated particle energy spectrum. This code has been continuously modified incorporating the improvements mentioned above. Recently, this code has been made available on the internet for use by all researchers (http://lheawww.gsfc.nasa.gov/users/ramaty/ViewPubs/ramaty.html). A thorough understanding of the nuclear physics underlying the code is essential for the proper use of the code

and for judging the significance and reliability of any result. The purpose of this paper is also to act as a companion document to the code itself, providing this understanding. Some of the discussion in this paper therefore specifically relates to this code.

In this paper we will describe the excitation functions, i.e., the total cross sections for the production of the various gamma-ray lines as a function of the energy of the energetic particle. In a subsequent paper we will deal with the other aspects of the nuclear physics relating to the gamma-ray line spectrum (e.g., the nuclear kinematics influencing the line shapes) and will describe in detail the calculation method of the computer code.

2. Line Production Cross Sections

In RKL the nuclear cross sections were constructed from laboratory data obtained using two complementary methods. In the first method, the cross section is directly derived by measuring the total yield of the gamma-ray line. We will refer to this method as the "gamma-ray method". In the second method, the cross section is inferred from measurements of the energy of the scattered particle after excitation of the target nuclei to various levels. The cross section for producing a given gamma-ray line is then obtained by summing the contributions to the line from the various levels according to known branching ratios. We will refer to this second method as the "recoil method". The first method is of course to be preferred. The gamma-ray method data used by RKL were from Foley et al. (1962a), Foley et al. (1962b) and Zobel et al. (1968). But these measurements were limited to only a few projectile energies, for only a few elements, at only one or at a very few angles, and were obtained with NaI detectors so that the lines were not adequately resolved from each other. In RKL, therefore, the recoil method was used most often.

The development of gamma-ray line astronomy motivated extensive and systematic laboratory measurements that were geared specifically to its needs. These gamma-ray method measurements (Dyer et al. 1981; Narayanswarmy et al. 1981; Seamster et al. 1984; Dyer et al. 1985; Lang et al. 1987; Lesko et al. 1988; Kiener et al. 1998) were performed with high-resolution Ge detectors and at many particle energies and angles and establish solid credibility for astronomical gamma-ray line spectroscopy.

The gamma-ray lines discussed in this paper are listed in Tables 1 through 6. The first column is the observed line energy in MeV, the second column gives the isotope and level transition responsible for the given line, the third column gives those reactions leading to the emission of the line (most of these reactions are discussed in this paper), and the last column gives the mean lifetime in seconds of the nuclear level or radioactive isotope. As will

be discussed, most lines were included because they were detected in laboratory gamma-ray measurements. Because these measurements involve inspection of the gamma-ray spectrum, this ensures that all of the strongest lines were identified and included. A small number of lines for which laboratory measurements are not available were included based on theoretical reasoning as will be discussed in the following sections. There are also many more weak lines resulting from transitions among the numerous bound states in nuclei heavier than ^{16}O. RKL treated these lines as an "unresolved" component. Since our treatment of these lines is entirely different from that of the strong lines presented in this paper, this "unresolved" component will be discussed in a subsequent paper.

In the following sections we discuss the excitation functions for lines from proton and α reactions with He, C, N, O, Ne, Mg, Al, Si, S, Ca and Fe. In addition to discussing cross sections that have changed and cross sections that have been added since RKL, for completeness we also include discussion of those cross sections that have not been changed.

2.1. Lines from Reactions on He

Interactions of α particles with ^{4}He produce lines at 0.429 and 0.478 MeV (Table 1). The astrophysical importance of these lines was first pointed out by Kozlovsky & Ramaty (1974). The 0.429 MeV line results from the deexcitation of the first excited state of ^{7}Be populated by the reaction ^{4}He(α,n)^{7}Be*. The 0.478 MeV line has two components: a prompt one, resulting from the deexcitation of the first excited state of ^{7}Li populated by the reaction ^{4}He(α,p)^{7}Li*, and a delayed one resulting from the decay of ^{7}Be through the ^{7}Li excited state. The mean life of ^{7}Be is 77 days and it decays 10.5% of the time to the first excited state of ^{7}Li.

In Figure 2a we show the cross section for the total (ground + excited state) ^{7}Li production and the cross section for the reaction ^{4}He(α,p)^{7}Li$^{*0.478}$. For the total ^{7}Li production the data are from Slobodrian & Conzett (1982) at 9.37 and 9.64 MeV nucleon^{-1}, from King et al. (1977) between 9.75 and 12.4 MeV nucleon^{-1}, and from the measurements and summary of Mercer et al. (2001) between 15 and 155 MeV nucleon^{-1}. The ^{7}Li$^{*0.478}$ cross section is from Slobodrian & Conzett (1982) at 9.64 MeV nucleon^{-1} and from King et al. (1977) between 9.75 and 12.4 MeV nucleon^{-1}. As there are no measurements at higher energies, we assumed that the ratio of the cross section for producing the first excited state to the total cross section is energy independent and has the value 0.3 based on measurements of this ratio at the highest four energies considered by King et al. (1977).

In Figure 2b we show the cross section for the total (ground + excited state) ^{7}Be

production. The data are from King et al. (1977) between 9.86 and 11.84 MeV nucleon^{-1}, and from the measurements and summary of Mercer et al. (2001) between 15 and 155 MeV nucleon^{-1}. We use 10.5% of this total ^{7}Be production cross section to calculate the delayed 0.478 MeV line. There are no cross section measurements for the reaction ^{4}He(α,n)^{7}Be$^{*0.429}$. We assume that the ratio of the cross section for producing the excited state to the total cross section for ^{7}Be is the same as for ^{7}Li at the same energy increment above the corresponding thresholds. The resulting cross section is also shown in Figure 2b.

Interactions of both ^{3}He nuclei and α particles with ^{4}He produce a line at 3.562 MeV resulting from deexcitations in ^{6}Li (Table 5). The cross section for the reaction ^{4}He(^{3}He,p)^{6}Li$^{*3.563}$ was measured by Harrison (1967) between 4.6 and 6.2 MeV nucleon^{-1}, by Koepke & Brown (1977) at 9.3 MeV nucleon^{-1}, and by Halbert et al. (1973) at 18 MeV nucleon^{-1} and 20.4 MeV nucleon^{-1}. At higher energies we extrapolated the cross section as expected for reactions with 2 particles in the exit channel. This cross section is shown in Figure 3. Also shown in Figure 3 is the total cross section for the reaction ^{4}He(^{3}He,p)^{6}Li(ground + excited states), taken from Ramaty et al. (2000b) where the sources of the data are detailed. We see that the cross section for producing the excited state is on average $\sim$10% of the total. Considering the production of 3.562 MeV gamma rays by α particles, we note that even though there are two channels for producing ^{6}Li in $\alpha\alpha$ reactions, ^{4}He(α,d)^{6}Li and ^{4}He(α,pn)^{6}Li, conservation of isotopic spin allows only the latter reaction to populate the 3.563 MeV excited state (Kozlovsky & Ramaty 1974). The cross section for this reaction is also shown in Figure 3, based on the (pn) data given by Mercer et al. (1997) between 15.36 and 39.6 MeV nucleon^{-1}. Between 49.6 and 154.9 MeV we employed the data of Mercer et al. (2001). However, since the contributions of the two channels were not separated in these latter data, we assumed that the contribution of the (pn) channel is 60% of the total based on the data of Mercer et al. (1997). Since there are no measurements of the cross section for the reaction ^{4}He(α,pn)^{6}Li$^{*3.563}$, we assumed that the ratio of this cross section to the total ^{6}Li production cross section via the (pn) channel is $\sim$10%, in analogy with the ratio between the excited state and total cross sections for the ^{3}He induced reactions, as pointed out above.

2.2. Lines from Reactions on ^{12}C

Several lines result from the bombardment of ^{12}C with protons and α particles. We first consider the gamma ray line at 4.438 MeV which results from deexcitations of ^{12}C (Table 5). We refer to such reactions as inelastic to distinguish them from spallation reactions in which the gamma-ray emitting nucleus is not the original target but results from the breakup of the target. The cross section for 4.438 MeV line production in proton induced reactions

from threshold to 23 MeV is from the gamma-ray method measurements of Dyer et al. (1981). From 23 to 200 MeV we use the cross sections given by RKL which were based on measurements of the recoiling protons. These cross sections are consistent with the gamma ray measurements of Lang et al. (1987) at 40, 65 and 85 MeV and Lesko et al. (1988) at 30, 33, 40 and 50 MeV. Above 200 MeV we extrapolate the cross section to coincide with the gamma ray measured value at 1 GeV (Alard et al. 1974). The resultant cross section is shown in Figure 4. We point out that because of kinematical Doppler broadening, the gamma-ray method cannot distinguish between photons resulting from the ^{12}C spallation reaction leading to ^{11}B$^{*4.445}$ (Table 5) and the inelastic reaction producing ^{12}C$^{*4.439}$. However, as pointed out by Lang et al. (1987), at 40 MeV ^{11}B$^{*4.444}$ production is negligible relative to the production of ^{12}C$^{*4.439}$. But at higher energies the relative contribution of the spallation reaction is expected to be larger, and this could explain the flattening of the cross section above 200 MeV contrary to the expected rapid decline of the inelastic ^{12}C$^{*4.439}$ producing reaction. For simplicity, above 200 MeV we assume that the two processes make equal contributions to the total cross section shown in Figure 4.

Also shown in Figure 4 is the cross section for the reaction ^{12}C(p,p$'$)^{12}C$^{*15.11}$ (Table 6), where the data are from Lang et al. (1987).

The cross section for 4.438 MeV line production in α-particle induced reactions is well measured by the gamma-ray method between 2 and 6.5 MeV nucleon^{-1} (Dyer et al. 1985). In addition, there are α-particle recoil measurements up to 10 MeV nucleon^{-1} (summarized in RKL) which agree quite well with the Dyer et al. (1985) data. There are no data at higher energies except the gamma ray measurement of Zobel et al. (1968) at 15 MeV nucleon^{-1} which is quite uncertain because the measurement was carried out at only one angle. We have extrapolated the cross section from 10 MeV nucleon^{-1} assuming an energy dependence similar to the proton induced cross section shown in Figure 4. The resulting cross section is also shown in Figure 4. We do not include the production of 15.10 MeV gamma rays by α-particle induced reactions because there are no data on the cross section.

In addition to the lines at 4.438 and 15.10 MeV resulting from inelastic reactions on ^{12}C, we also include the lines at 3.684 and 3.853 MeV (Table 5) produced by similar reactions of protons and α particles with ^{13}C. For both protons and α particles the cross sections for these reactions were estimated by RKL to be 90% and 20%, respectively, of the cross section for producing the 4.438 MeV line. We do not show these cross sections in a figure but the lines were included in the gamma ray production code referred to in the Introduction (§1) by taking a ^{13}C/^{12}C abundance ratio of 0.011 (Firestone & Shirley 1996).

Interactions of α particles with ^{12}C also produce lines at 5.269 and 5.240 MeV via the fusion reactions ^{12}C(α,p$\gamma_{5.269}$)^{15}N and ^{12}C(α,n$\gamma_{5.240}$)^{15}O as given in Table 6. Dyer et al.

(1985) measured the combined cross section for these reactions at 5 and 6.75 MeV nucleon^{-1}. The combined cross section shown in Figure 5 is based on these data, the expected behavior near threshold and an extrapolation to high energies based on the expected behavior for reactions with 2 particles in the exit channel. In our calculations we assume equal cross sections for the two reactions.

Spallation reactions of ^{12}C produce lines at 0.718, 1.022, 2.000, 2.124, 6.337, 6.476, 6.741 and 6.790 MeV from ^{10}B, ^{11}B and ^{11}C as given in Tables 1, 2, 3 and 6. Lang et al. (1987) measured the cross sections for the reactions ^{12}C(p,x$\gamma_{2.000}$)^{11}C and ^{12}C(p,2p$\gamma_{2.124}$)^{11}B at 40, 65 and 85 MeV. The combined cross section shown in Figure 5 is based on these data, where at low energies we extrapolated to the thresholds of the reactions and at high energies we continued the trend established by the measurements. The ratio of the cross sections for the reactions ^{12}C(p,x$\gamma_{2.000}$)^{11}C and ^{12}C(p,2p$\gamma_{2.124}$)^{11}B is very nearly energy independent and equal to about 2 (Lang et al. 1987). Also shown in Figure 5 is the cross section for the reaction ^{12}C(p,x$\gamma_{0.718}$)^{10}B taken from RKL. We assume that the cross section for the reaction ^{12}C(p,x$\gamma_{1.022}$)^{10}B is the same as that given in RKL, i.e., it has the same energy dependence as that of the 0.718 MeV line and normalized at 40% of that cross section.

As in RKL, we assume that the sum of the cross sections for producing the 6.337, 6.476, 6.741 and 6.790 MeV lines by both protons and α particles is 25% of the sum of the cross sections for producing the lines at 5.105, 5.180, 5.241, 5.270 and 5.298 in interactions of protons and α particles, respectively, with ^{16}O. These lines from ^{16}O spallation are discussed in §2.4. We further assume that the cross section for producing each of the 4 lines at 6.337, 6.476, 6.741 and 6.790 MeV is 25% of the total as in RKL.

2.3. Lines from Reactions of ^{14}N

The strongest lines resulting from inelastic reactions of ^{14}N are at 1.635, 2.313 and 5.105 MeV (Tables 3, 4 and 5). The cross sections of the reactions ^{14}N(p,p$'\gamma_{2.313}$)^{14}N and ^{14}N(p,p$'\gamma_{1.635}$)^{14}N were measured by the gamma-ray method from 4 to 23 MeV by Dyer et al. (1981), at 30, 33 and 40 MeV by Lesko et al. (1988), and at 120 MeV by Clegg et al. (1961). These cross sections are shown in Figure 6. The cross section for producing the 2.313 MeV line includes the cross section of the reaction ^{14}N(p,n)^{14}O(e$^+$,ϵ)^{14}N$^{*2.313}$. The halflife of ^{14}O (71 s) is short enough to include its contribution to 2.313 MeV line production in calculations of prompt deexcitation gamma ray line production. In §2.10 we present calculations of delayed gamma ray line emission from radioisotopes of much longer half life. The cross section for the reaction ^{14}N(p,p$'\gamma_{5.105}$)^{14}N above 8 MeV is assumed to be 70% of the cross section for the reaction ^{14}N(p,p$'\gamma_{2.313}$)^{14}N as in RKL. Below 8 MeV we assume

the typical behavior near the threshold of ∼5.5 MeV. The cross section for the reaction ^{14}N(p,p′$\gamma_{5.105}$)^{14}N is also shown in Figure 6.

The cross sections for the reactions ^{14}N(α,$\alpha'\gamma_{2.313}$)^{14}N and ^{14}N(α,$\alpha'\gamma_{1.635}$)^{14}N were measured by the gamma-ray method from 2 to 6.5 MeV nucleon^{-1} by Dyer et al. (1985). We extrapolated to higher energies by following the trend established at lower energies, with a ratio of 0.6 between the two cross sections. These cross sections are also shown in Figure 6. We assume that the cross section of the reaction ^{14}N(α,$\alpha'\gamma_{5.105}$)^{14}N is 70% of the cross section of the reaction ^{14}N(α,$\alpha'\gamma_{2.313}$)^{14}N as in RKL, neglecting the small threshold difference.

The strongest line from ^{14}N spallation reactions is the 4.438 MeV line of ^{12}C with an additional contribution from the 4.444 MeV line of ^{11}B (Table 5). The cross section for the production of the ∼4.44 MeV line from proton interactions with ^{14}N was measured only at 120 MeV by Clegg et al. (1961) and was found to be 2.4 times the cross section for the reaction ^{16}O(p,x$\gamma_{4.438}$)^{12}C at the same energy. We thus employ 2.4 times the cross section for the reaction ^{16}O(p,x$\gamma_{4.438}$)^{12}C presented in §2.4. In the absence of data for the corresponding α-induced reactions, we adopted a similar approach, i.e. we simply employed the cross section for the reaction ^{16}O(α,x$\gamma_{4.438}$)^{12}C, also presented in §2.4, without any renormalization.

2.4. Lines from Reactions of ^{16}O

Proton and α-particle induced inelastic reactions on ^{16}O produce lines at 2.742, 6.129, 6.916 and 7.115 MeV as given in Tables 4 and 6. The cross section for the reaction ^{16}O(p,p′$\gamma_{6.129}$)^{16}O was measured by the gamma-ray method by Dyer et al. (1981) between 8 and 23 MeV, by Narayanswarmy et al. (1981) at 23.7 and 44.6 MeV, by Lang et al. (1987) at 40, 65 and 85 MeV, and by Lesko et al. (1988) at 30, 33, 40 and 50 MeV. At 135 MeV we used the evaluation of Lang et al. (1987) based on recoil proton data. Averaging over all these data we obtained the cross section shown in Figure 7. At high energies this curve continues the trend established by the measurements at lower energies. The cross section for the reaction ^{16}O(α,$\alpha'\gamma_{6.129}$)^{16}O is also shown in Figure 7. It was measured by the gamma-ray method by Dyer et al. (1985) from threshold to 6.5 MeV nucleon^{-1}. Between 6.5 and 40 MeV nucleon^{-1} we used the calculations of Tatischeff et al. (1996). We have extrapolated the cross section to higher energies assuming an energy dependence similar to the proton induced cross section shown in Figure 7.

The cross section for the reaction ^{16}O(p,p′$\gamma_{2.742}$)^{16}O, shown in Figure 7, was measured by the gamma-ray method by Kiener et al. (1998) from threshold to 19 MeV. Between 20 and 30 MeV we used the calculations of RKL based on recoil proton data. At higher

energies we extrapolated the cross section following the trend shown by the cross section for the 6.129 MeV line. The data of Lang et al. (1987) at 40 and 65 MeV are consistent with this extrapolation, however they appear to be somewhat high at 85 MeV. In both cross section measurements of Zobel et al. (1968) and Dyer et al. (1985) of reactions induced by α particles in ^{16}O, the 2.742 MeV line was not seen. This is consistent with the fact that parity conservation would prevent the excitation by α particles of the 8.872 MeV level, which leads to the 2.742 MeV line by deexciting to the 6.130 MeV level (Table 6). Thus we do not include production of the 2.742 MeV line by α particles.

The cross sections for the reactions ^{16}O(p,p$'\gamma_{6.916}$)^{16}O and ^{16}O(p,p$'\gamma_{7.115}$)^{16}O are shown in Figure 8. They were measured by the gamma-ray method from threshold to 19 MeV by Kiener et al. (1998). Between 20 and 40 MeV we used the calculations of Tatischeff et al. (1996). Using the gamma-ray method, Zobel et al. (1968) measured cross sections for a feature around 7 MeV for proton energies between 12 and 145 MeV. Because of the energy resolution of the NaI detector used, these measurements included contributions from both the 6.916 and 7.115 MeV lines and also a line at 7.299 MeV resulting from ^{16}O spallation. Up to 40 MeV we attribute the difference between the Zobel et al. (1968) cross sections and those determined for the 6.916 and 7.115 MeV lines to the contribution of the 7.299 MeV line. Above 40 MeV we assumed that the three lines make equal contributions to the cross sections measured by Zobel et al. (1968).

The cross sections for the reactions ^{16}O(α,$\alpha'\gamma_{6.916}$)^{16}O and ^{16}O(α,$\alpha'\gamma_{7.115}$)^{16}O are also shown in Figure 8. These cross sections were measured using the gamma-ray method by Dyer et al. (1985) from threshold to 6.5 MeV nucleon^{-1} and calculated by Tatischeff et al. (1996) up to 40 MeV nucleon^{-1}. We have extrapolated the cross sections to higher energies assuming an energy dependence similar to the proton induced cross section shown in Figure 8. Unlike proton-induced reactions producing the 3 lines at 6.916, 7.115 and 7.299 MeV that were measured as a single feature by Zobel et al. (1968) between 12 and 145 MeV, for α-particle induced reactions there is only one equivalent measurement at 13 MeV nucleon^{-1}. Combining this measurement with the calculations of Tatischeff et al. (1996), we obtain a cross section of 2 mb at 13 MeV nucleon^{-1} for the 7.299 MeV line. We extrapolated this value to higher energies by assuming that asymptotically the cross sections for the production of the three lines are equal.

The lines from spallation reactions of ^{16}O are at 0.718, 1.022, 1.635, 2.313, 3.684, 3.853, 4.438, 5.105, 5.180, 5.240, 5.269, 5.298, 6.175, 6.322 and 7.299 MeV as given in Table 1. The cross section for the reaction ^{16}O(p,x$\gamma_{4.438}$)^{12}C was measured by the gamma-ray method by Dyer et al. (1981) from 14 to 23 MeV, by Lesko et al. (1988) at 30, 33, 40 and 50 MeV, by Foley et al. (1962b) at 150 MeV, and by Alard et al. (1974) at 1 GeV. Averaging

over these data above 23 MeV we obtained the cross section shown in Figure 9. The cross section for the reaction ^{16}O(α,x$\gamma_{4.438}$)^{12}C was also measured by the gamma-ray method by Dyer et al. (1985) between 5.5 and 6.5 MeV nucleon^{-1} and Zobel et al. (1968) at 13 MeV nucleon^{-1}. The latter measurement, however, is uncertain because it was made at only one angle. At higher energies we assumed an energy dependence similar to that of the ^{16}O(p,x$\gamma_{4.438}$)^{12}C reaction, resulting in the cross section shown in Figure 9. We ignore the reaction ^{16}O(p,x,$\gamma_{15.11}$)^{12}C since its cross section is less than 1 mb (Lang et al. 1987).

The cross sections for the reactions ^{16}O(p,x$\gamma_{5.269}$)^{15}N and ^{16}O(p,x$\gamma_{5.240}$)^{15}O were measured by the gamma-ray method at 30, 33 and 40 MeV (Lesko et al. 1988) and at 40, 65 and 85 MeV (Lang et al. 1987). These lines are due to transitions to the ground state from the first excited level in ^{15}N and the second excited level in ^{15}O. Additional lines at 5.298 MeV are expected from the second excited level in ^{15}N and at 5.180 MeV from the first excited level in ^{15}O. Another spallation reaction of ^{16}O leading to a line in this energy region is ^{16}O(p,x$\gamma_{5.105}$)^{14}N for which the cross section was also measured by Lang et al. (1987) at 40, 65 and 85 MeV. Lang et al. (1987) also provided the total combined cross section for these 5 lines at 40, 65 and 85 MeV. Based on all these data and the upper limit of 15 mb at 23 MeV (Dyer et al. 1981) we constructed the total combined cross section, shown in Figure 9, where at high energies we followed the trend of the cross section for the reaction ^{16}O(p,x$\gamma_{4.438}$)^{12}C. Based on the data of Lang et al. (1987), we assign partial cross sections of 18%, 28%, 12%, 21% and 21% of the total ∼5.2 MeV line cross section for the 5.269, 5.240, 5.105, 5.298 and 5.180 MeV lines, respectively. The cross section for the production of these 5 lines by α particle interactions with ^{16}O was measured by the gamma-ray method at only one energy (13 MeV nucleon^{-1}) by Zobel et al. (1968), without resolving the individual lines. We constructed the total cross section shown in Figure 9 using this measurement, extrapolating at low energies to the threshold. At high energies we assumed a relationship between the ∼5.2 and 4.438 MeV line production cross sections by α particles similar to the relationship between the corresponding cross sections in proton induced reactions. In addition, for the partial cross sections of the 5 lines we assumed the same fractions as for the proton induced reactions given above.

The derivation of the cross sections for the reactions ^{16}O(p,2p$\gamma_{7.299}$)^{15}N and ^{16}O(α,αp$\gamma_{7.299}$)^{15}N was discussed above, in connection with the reactions producing the 6.916 and 7.115 MeV lines. The resulting cross sections are shown in Figure 10.

We have adopted a similar approach for the reactions ^{16}O(p,x$\gamma_{6.175}$)^{15}O and ^{16}O(p,2p$\gamma_{6.322}$)^{15}N. There are no direct measurements of the cross sections of these reactions. Using the gamma-ray method, the cross section for a feature at ∼6.2 MeV was measured at proton energies of 12, 28, 48 and 145 MeV (Zobel et al. 1968) and 1 GeV (Alard et al. 1974). However,

these measurements did not resolve the three lines at 6.129, 6.175 and 6.322 MeV which contribute to this feature. Thus we constructed the combined cross section for the 6.175 and 6.322 MeV producing reactions by subtracting from the data of Zobel et al. (1968) and Alard et al. (1974) the cross section for producing the 6.129 MeV line shown in Figure 7. However, since Narayanswarmy et al. (1981) did not observe the 6.322 MeV line at 44 MeV, below 100 MeV we approximated the cross section as shown in Figure 10. We took the 6.175 MeV and 6.322 MeV line cross sections to be 1/3 and 2/3 of the combined cross section, based on the data of Goryachev et al. (1973).

There are no measurements of the cross sections for producing the 6.175 and 6.322 MeV lines in α particles interactions with ^{16}O except one measurement of the combined $\sim$6.2 MeV feature at 13 MeV nucleon^{-1} by Zobel et al. (1968). This cross section is very close to the cross section for producing 6.129 MeV line shown in Figure 7, indicating a small value for the combined cross section for producing the 6.175 and 6.322 MeV lines, on the order of the cross section for the reaction ^{16}O(α,x$\gamma_{7.299}$)^{15}N shown in Figure 10. We thus assume that the combined cross section for the reactions ^{16}O(α,x$\gamma_{6.175}$)^{15}O+ ^{16}O(α,x$\gamma_{6.322}$)^{15}N is the same as the cross section for the reaction ^{16}O(α,x$\gamma_{7.299}$)^{15}N shown in Figure 10. We assumed the same ratio for the production of the 6.175 MeV and 6.322 MeV lines as in the proton induced reactions mentioned above.

The lines at 1.635 and 2.313 MeV result from deexcitations in ^{14}N produced by spallation of ^{16}O. The cross section for the reaction ^{16}O(p,x$\gamma_{2.313}$)^{14}N was measured by the gamma-ray method at 28, 48 and 145 MeV by Zobel et al. (1968) and at 40, 65 and 85 MeV by Lang et al. (1987). Based on these data we constructed the cross section shown in Figure 10. There are no data on the production of the 1.635 MeV line. Using the average ratio between the production of the 1.635 and 2.313 MeV lines in inelastic interactions of ^{14}N (§2.3), we take the cross section for the reaction ^{16}O(p,x$\gamma_{1.635}$)^{14}N to be 60% of the cross section for producing the 2.313 MeV line.

The lines at 0.718 and 1.022 MeV result from deexcitations in ^{10}B produced by spallation of ^{16}O. The cross sections for the reactions ^{16}O(p,x$\gamma_{0.718}$)^{10}B and ^{16}O(p,x$\gamma_{1.022}$)^{10}B were only measured at 150 MeV by Foley et al. (1962b). At this energy the two cross sections are about equal and 60% of the cross section for the reaction ^{12}C(p,x$\gamma_{0.718}$)^{10}B at the same energy (Figure 5). In the absence of more data, at all energies we take the cross section for the reactions ^{16}O(p,x$\gamma_{0.718}$)^{10}B and ^{16}O(p,x$\gamma_{1.022}$)^{10}B to be 60% of the ^{12}C(p,x$\gamma_{0.718}$)^{10}B spallation reaction. The lines at 3.684 MeV and 3.853 MeV result from deexcitations in ^{13}C also produced by spallation of ^{16}O. Zobel et al. (1968) measured by the gamma-ray method the cross section for a feature at 3.72 MeV which most likely is the combined cross section for the reactions ^{16}O(p,x$\gamma_{3.684}$)^{13}C and ^{16}O(p,x$\gamma_{3.853}$)^{13}C. These measurements were carried out

at 28, 48 and 145 MeV. Based on these data and the expected behavior near the threshold, we have constructed the cross section shown in Figure 10. As for the production of these lines in inelastic interactions (§2.2), we take the ratio between the above two cross sections to be 4.5.

In addition to proton and α-particle induced reactions with ^{16}O, the reaction ^{16}O(^{3}He,p)^{18}F* leads to very strong line emission at 0.937, 1.042 and 1.081 MeV (Tables 1 and 2). The importance of these lines as a diagnostic for accelerated ^{3}He was pointed out by Mandzhavidze et al. (1997). The cross sections for the production of these lines were measured by the gamma-ray method from 0.9 to 1.3 MeV nucleon^{-1} (Hegg et al. 1980). At higher energies, up to about 3.5 MeV nucleon^{-1} there are only data on the total cross section (Hahn & Ricci 1966) and there are no data at higher energies. As the maximum cross section is already reached at about 2 MeV nucleon^{-1}, we extrapolated to higher energies assuming the expected behavior of reactions with 2 bodies in the final state. The total cross section for the three lines is shown in Figure 11. As can be seen, the cross section extends to very low energies due to the fact that the reactions are exothermic. We assume that the ratios of the partial cross sections are energy independent and equal to average values measured by Hegg et al. (1980). We took 47%, 35% and 18% of the total cross section for the 0.937, 1.042 and 1.081 MeV lines, respectively.

2.5. Lines from Reactions on Ne

Inelastic reactions of ^{20}Ne produce lines at 1.634, 2.614 and 3.333 MeV as given in Tables 3 and 4. The cross section for the reaction ^{20}Ne(p,p$'\gamma_{1.634}$)^{20}Ne from 2 to 24 MeV was measured by the gamma-ray method (Dyer et al. 1981). We extrapolated to higher energy assuming a trend similar to other inelastic cross sections discussed above. The resultant cross section is shown in Figure 12. The cross sections for the reactions ^{20}Ne(p,p$'\gamma_{2.614}$)^{20}Ne and ^{20}Ne(p,p$'\gamma_{3.333}$)^{20}Ne were found at 17 MeV to be 25% and 10%, respectively, of the cross section for the reaction ^{20}Ne(p,p$'\gamma_{1.634}$)^{20}Ne (Schrank et al 1962). We assumed that these ratios pertain at all energies above 12 MeV, that the cross sections exhibit the typical decrease toward the higher thresholds, and that the ratio between the cross sections for producing the 2.614 and 3.333 MeV lines is constant at all energies as in RKL. The cross section for the reaction ^{20}Ne(p,p$'\gamma_{2.614}$)^{20}Ne is shown in Figure 12.

The cross section for the reaction ^{20}Ne(α,$\alpha'\gamma_{1.634}$)^{20}Ne was measured by the gamma-ray method from 1.25 to 6.5 MeV nucleon^{-1} (Seamster et al. 1984). At 9.5 MeV nucleon^{-1} RKL calculated the cross section using α-particle recoil data (Seidlitz et al 1958). We extrapolated to higher energy assuming a trend similar to other inelastic cross sections

discussed above. The cross section is shown in Figure 12. The cross section for the reaction ^{20}Ne(α,$\alpha'\gamma_{2.614}$)^{20}Ne was measured by the gamma-ray method from 2 to 4.25 MeV nucleon^{-1} (Seamster et al. 1984). We again extrapolated to higher energies assuming a trend similar to other inelastic cross sections. This cross section is also shown in Figure 12. As for the proton induced reactions, we take the cross section for the reaction ^{20}Ne(α,$\alpha'\gamma_{3.333}$)^{20}Ne to be 40% of the cross section for the reaction ^{20}Ne(α,$\alpha'\gamma_{2.614}$)^{20}Ne and further assume that this ratio is energy independent.

The strongest line from inelastic reactions of ^{22}Ne is at 1.275 MeV (Table 2). Based on proton recoil measurements from near threshold to 24.5 MeV, RKL concluded that the cross section for producing this line is approximately 67% of that for producing the 1.634 MeV line in ^{20}Ne and suggested applying this ratio at all energies. RKL also suggested using the same procedure for the corresponding α-particle induced reactions. We thus include the 1.275 MeV line from protons and from α particles by using the cross sections for the reactions ^{20}Ne(p,p$'\gamma_{1.634}$)^{20}Ne and ^{20}Ne(α,$\alpha'\gamma_{1.634}$)^{20}Ne (Figure 12), respectively, both scaled by 0.67 and by the ^{22}Ne/^{20}Ne abundance ratio of 0.10 (Firestone & Shirley 1996).

Interactions of α particles with ^{20}Ne produce ^{23}Na via fusion. The cross section for the reaction ^{20}Ne(α,p$\gamma_{2.263}$)^{23}Na (Table 4) was measured from 2 to 6.5 MeV nucleon^{-1} by (Seamster et al. 1984). At higher energies we assume the behavior typical for reactions with 2 bodies in the final state. The resulting cross section is shown in Figure 13. The 2.263 MeV line should be accompanied by a line at 0.440 MeV with a cross section for the reaction ^{20}Ne(α,p$\gamma_{0.440}$)^{23}Na (Table 1) that is at least as large as that for producing the 2.263 MeV line. Since there are no data for the former, we assumed equal cross sections for both lines.

The only line produced by ^{20}Ne spallation for which cross section measurements are available is the 6.129 MeV line of ^{16}O (Table 6). The cross section for the reaction ^{20}Ne(p,x$\gamma_{6.129}$)^{16}O was measured by the gamma-ray method from 17 to 23 MeV (Dyer et al. 1981). We show this cross section in Figure 13, where above 23 MeV we assume the same shape as that of the cross section for the reaction ^{16}O(p,x$\gamma_{4.438}$)^{12}C (Figure 9).

RKL have pointed out that the other strong lines resulting from ^{20}Ne spallation by protons are expected from deexcitation of the first two excited states in ^{19}Ne and ^{19}F at 0.110, 0.197, 0.238, and 0.275 (Table 1), in analogy with the cluster of ^{16}O spallation lines at 5.180, 5.240, 5.298 and 5.269 MeV (Table 6). We thus take the sum of the cross sections for the four ^{20}Ne spallation lines to be 88% of the cross section for ^{16}O(p,x$\gamma_{5.2}$)^{14}N,^{15}N,^{15}O shown in Figure 9, because the contribution of the 5.105 MeV ^{14}N line is 12% of the total (§2.4). For simplicity we further assume equal partial cross sections for the 4 lines.

2.6. Lines from Reactions of Mg

The strongest line produced by inelastic reactions on ^{24}Mg is at 1.369 MeV resulting from transitions from the first excited state to the ground state (Table 2). The cross section for the reaction ^{24}Mg(p,p$'\gamma_{1.369}$)^{24}Mg from 2.1 to 23 MeV was measured by the gamma-ray method (Dyer et al. 1981). These measurements were made using pure ^{24}Mg, but the higher energy cross section measurements from 9 to 50 MeV (Lesko et al. 1988) and at 143 MeV (Foley et al. 1962a) were made using natural Mg. In Figure 14 we combine these measurements of the cross section for producing the 1.369 MeV line consistently for a target of pure ^{24}Mg: below 9 MeV, the threshold for the reaction ^{25}Mg(p,x$\gamma_{1.369}$)^{24}Mg, we use the Dyer et al. (1981) data while at higher energies we use the Lesko et al. (1988) and Foley et al. (1962a) data, increased by a factor of 1.27, the ratio of natural Mg to pure ^{24}Mg (Firestone & Shirley 1996). We extrapolated above 143 MeV following the trend established by the measurements.

RKL provided arguments that show that the expected next strongest line from inelastic reactions on ^{24}Mg is at 2.754 MeV resulting from transitions from the second to the first excited state (Table 4), with a cross section that is about 10% of the cross section for ^{24}Mg(p,p$'\gamma_{1.369}$)^{24}Mg. We assume that this percentage remains valid for natural Mg. We thus take the cross section for the total production of the 2.754 MeV line to be 10% of the cross section for the reaction ^{24}Mg(p,p$'\gamma_{1.369}$)^{24}Mg.

The cross section for the reaction ^{24}Mg(α,$\alpha'\gamma_{1.369}$)^{24}Mg was measured by the gamma-ray method from 2 to 6.5 MeV nucleon^{-1} by Seamster et al. (1984). At 10 MeV nucleon^{-1} RKL calculated the cross section using α-particle recoil data (Janus & McCarthy 1974). We extrapolated to higher energy assuming a trend similar to other inelastic cross sections discussed above. The cross section is shown in Figure 14. The cross section for the reaction ^{24}Mg(α,$\alpha'\gamma_{2.754}$)^{24}Mg was taken to be 10% of the cross section for ^{24}Mg(α,$\alpha'\gamma_{1.369}$)^{24}Mg similar to the corresponding proton reactions discussed above.

We include a line from the isotope ^{26}Mg: ^{26}Mg(p,p$'\gamma_{1.809}$)^{26}Mg. As in RKL, we assume that the cross section is 50% of the cross section for ^{24}Mg(p,p$'\gamma_{1.369}$)^{24}Mg. Similarly, the cross section for ^{26}Mg(α,$\alpha'\gamma_{1.809}$)^{26}Mg is assumed to be 50% of the cross section for ^{24}Mg(α,$\alpha'\gamma_{1.369}$)^{24}Mg.

The strongest spallation lines from Mg isotopes are at 1.634 and 1.636 MeV from ^{20}Ne and ^{23}Na, respectively. The cross section for producing $\sim$1.63 MeV gamma rays by protons was measured by the gamma-ray method by Lesko et al. (1988) with a natural Mg target from 9 to 50 MeV. At higher energies, we used the measurement of Foley et al. (1962a) at 143 MeV with natural Mg as well. In Figure 14 we show the cross section producing these

lines renormalized for a pure ^{24}Mg target by increasing these measurements by 1.27, the ratio of natural Mg to pure ^{24}Mg (Firestone & Shirley 1996). We do not use the measurements of Dyer et al. (1981) since they used pure ^{24}Mg and so did not include contribution to these lines from other isotopes. In particular, the strong reaction ^{26}Mg(p,$\alpha\gamma_{1.636}$)^{23}Na has a low threshold of ∼4 MeV. This is evident in that at 9 MeV, Lesko et al. (1988) measured a significant cross section whereas Dyer et al. (1981) reported none.

Other lines produced by spallation of Mg shown in the Tables are at 0.440, 0.451, 0.891, 1.600, 2.614 and 2.640 MeV. The cross section for the combined reactions ^{24}Mg(p,x$\gamma_{2.614}$)^{20}Ne and ^{24}Mg(p,x$\gamma_{2.640}$)^{23}Na was assumed to be 90% of the cross section for the reaction ^{24}Mg(p,x$\gamma_{\sim 1.63}$) above, based on the measurement of Zobel et al. (1968) at 30 MeV and of Foley et al. (1962a) at 143 MeV. Following RKL, we assume that the cross sections for the reactions ^{24}Mg(p,x$\gamma_{1.600}$)^{23}Mg, ^{24}Mg(p,x$\gamma_{0.440}$)^{23}Na, ^{24}Mg(p,x$\gamma_{0.451}$)^{23}Mg and ^{24}Mg(p,x$\gamma_{0.891}$)^{22}Na are 1/3, 1/2, 1/3 and 1/3 of the cross section for the reaction ^{24}Mg(p,x$\gamma_{\sim 1.63}$) above, respectively.

The combined cross section for producing the 1.634 and 1.636 MeV lines from the reactions ^{24}Mg(α, 2$\alpha\gamma_{1.634}$)^{20}Ne and ^{24}Mg(α, x$\gamma_{1.636}$)^{23}Na from 5.25 to 6.5 MeV nucleon^{-1} is from Seamster et al. (1984). The cross section at higher energies was constructed as follows: the shape of the cross section was taken to be similar to the cross section for the analogous (p,pα) reaction and the ratio of its maximum to the maximum of the (p,pα) reaction was taken to be the same as that of the ^{16}O(α,2α) and ^{16}O(p,pα) reactions. The cross section is shown in Figure 14.

The cross section for the reaction ^{24}Mg(α,p$\gamma_{2.211}$)^{27}Al from 2 to 6.5 MeV nucleon^{-1} is from Seamster et al. (1984). At higher energies we assume the usual behavior of (α,p) reactions. The cross section is shown in Figure 14.

2.7. Lines from Reactions of Si

The strongest line produced by inelastic reactions on ^{28}Si is at 1.779 MeV resulting from transitions from the first excited state to the ground state. The cross section for the reaction ^{28}Si(p,p′$\gamma_{1.779}$)^{28}Si from 4 to 23 MeV is from Dyer et al. (1981). In the range 30 to 50 MeV, it is from Lesko et al. (1988) and at 141 MeV it is from Foley et al. (1962a). All of these measurements used the gamma-ray method and natural Si targets. The Dyer et al. (1981) and Lesko et al. (1988) measurements are consistent at those energies where they overlap. The cross section is shown in Figure 15 where we increased the measured data by a factor of 1.08, the ratio of natural Si to pure ^{28}Si (Firestone & Shirley 1996).

The cross section for the reaction ^{28}Si(p,p′$\gamma_{6.879}$)^{28}Si was taken to be 13% of the cross

section for ^{28}Si(p,p$'\gamma_{1.779}$)^{28}Si as in RKL but cut off below the threshold of ∼7 Mev. The cross section for the reaction ^{28}Si(p,p$'\gamma_{5.099}$)^{28}Si was taken to be 50% of the cross section for ^{28}Si(p,p$'\gamma_{6.879}$)^{28}Si following RKL.

The cross section for the reaction ^{28}Si(α,$\alpha'\gamma_{1.779}$)^{28}Si from 1.75 MeV nucleon^{-1} to 6.5 MeV nucleon^{-1} is from Seamster et al. (1984). At higher energies we assume the usual inelastic behavior. The cross section is shown in Figure 15 where we increased the measured data by a factor of 1.08, the ratio of natural Si to pure ^{28}Si (Firestone & Shirley 1996).

The cross section for the reaction ^{28}Si(α,$\alpha'\gamma_{6.878}$)^{28}Si is assumed to be 13% of the cross section for ^{28}Si(α,$\alpha'\gamma_{1.779}$)^{28}Si as in RKL but cut off below the threshold of ∼1.75 MeV nucleon^{-1}. The cross section for the reaction ^{28}Si(α,$\alpha'\gamma_{5.099}$)^{28}Si is assumed to be 50% of the cross section for ^{28}Si(α,$\alpha'\gamma_{6.879}$)^{28}Si as in RKL.

The strongest spallation line from Si is at 1.369 MeV from ^{24}Mg. The cross section for producing this line from proton interactions was measured by the gamma-ray method with natural Si from 20 to 50 MeV by Lesko et al. (1988) and at 141 MeV by Foley et al. (1962a). The cross section is shown in Figure 15 where we increased the measured data by a factor of 1.08, the ratio of natural Si to pure ^{28}Si (Firestone & Shirley 1996).

Spallation of ^{28}Si produces lines at 0.781 and 0.957 MeV from ^{27}Si and 0.844 and 1.014 MeV from ^{27}Al as shown in the Tables. These lines were observed and measured by Lesko et al. (1988) from 9 to 50 MeV and Foley et al. (1962a) at 141 MeV by the gamma-ray method with natural Si target. The energy dependence of the measured cross sections are all very similar to that of the 1.369 MeV spallation line from Si described above. The ratios of the average cross sections of these lines to that of the 1.369 MeV spallation line are 16%, 21%, 26% and 39%, respectively.

Other spallation lines of ^{28}Si are at 1.634 and 2.614 MeV from ^{20}Ne, 2.211 from ^{27}Al and 2.164 MeV from ^{27}Si as shown in the Tables. These lines were only measured by Foley et al. (1962a) at 141 MeV. Foley et al. (1962a) did not separately measure the last two lines. We approximate the cross sections for these four lines by assuming an energy dependence similar to that of the other spallation lines and with ratios relative to the 1.369 MeV spallation line of 65%, 42%, 13% and 13% taken from Foley et al. (1962a).

In addition to these spallation lines, we have included the strong lines resulting from the reactions ^{28}Si(α,p$\gamma_{2.234}$)^{31}P, ^{28}Si(α,2p$\gamma_{2.235}$)^{30}Si and ^{28}Si(α,p$\gamma_{1.266}$)^{31}P. The combined cross section for the reactions ^{28}Si(α,p$\gamma_{2.234}$)^{31}P and ^{28}Si(α,2p$\gamma_{2.235}$)^{30}Si from 1.75 to 6.5 MeV nucleon^{-1} is from Seamster et al. (1984). At higher energies we assume the usual behavior of (α,p) reactions. The cross section for the reaction ^{28}Si(α,p$\gamma_{1.266}$)^{31}P from 2 to 6.5 MeV nucleon^{-1} is from Seamster et al. (1984). At higher energies we assume the usual behavior

of (α,p) reactions. The cross sections for production of these lines are shown in Figure 16 where we increased the measured data by a factor of 1.08, the ratio of natural Si to pure ^{28}Si (Firestone & Shirley 1996).

2.8. Lines from Reactions of Al, S and Ca

The abundances of Al, S and Ca are an order of magnitude less than the more abundant elements. We include only the strongest lines.

According to Lesko et al. (1988), the strongest lines from proton reactions with ^{27}Al are at 1.014 MeV from the inelastic reaction ^{27}Al(p,p$'\gamma_{1.104}$)^{27}Al and at 1.809 from the spallation reaction ^{27}Al(p,x$\gamma_{1.809}$)^{26}Mg. Their results show that the cross section for the first reaction has a similar energy dependence as that of the 0.847 MeV line from ^{56}Fe but with 24% of its magnitude. They also show that the cross section for the second reaction has an energy dependence similar to that of the 0.931 MeV spallation line from ^{26}Fe but with 50% of its yield. The strongest line resulting from α interactions with ^{27}Al is a doublet comprised of a line at 2.211 MeV resulting from ^{27}Al(α,$\alpha'\gamma_{2.211}$)^{27}Al and a line at 2.235 MeV from ^{27}Al(α,x$\gamma_{2.235}$)^{30}Si. The combined cross section for these reactions from 1.25 to 6.5 MeV nucleon^{-1} is from Seamster et al. (1984). At higher energies we assume the usual behavior for reactions with 2 bodies in the exit channel. The cross section is shown in Figure 16.

The strongest line from inelastic interactions of S is at 2.230 MeV from the deexcitation of the first excited state. According to Foley et al. (1962a), the cross section for the reaction ^{32}S(p,p$'\gamma_{2.230}$)^{32}S at $\sim$140 MeV is as large as the corresponding cross section for ^{24}Mg(p,p$'\gamma_{1.369}$)^{24}Mg. We assume this is true at all energies since the nuclear structure of ^{32}S is similar to the other elements composed of a whole number of alpha particles (e.g., ^{20}Ne, ^{24}Mg and ^{28}Si). We also assume that the cross section for the reaction ^{32}S($\alpha, \alpha'\gamma_{2.230}$)^{32}S is equal to the cross section for ^{24}Mg($\alpha, \alpha'\gamma_{1.369}$)^{24}Mg.

Spallation reaction of ^{32}S produce lines at 1.249, 1.266, 1.779, 2.029, 2.034, 2.232 and 2.234 MeV as shown in the Tables. The cross sections for the reactions ^{32}S(p,x$\gamma_{1.249}$)^{31}S, ^{32}S(p,x$\gamma_{1.266}$)^{31}P, ^{32}S(p,x$\gamma_{1.779}$)^{28}Si, ^{32}S(p,x$\gamma_{2.029}$)^{31}P, ^{32}S(p,x$\gamma_{2.034}$)^{31}S, ^{32}S(p,x$\gamma_{2.232}$)^{31}S and ^{32}S(p,$\gamma_{2.234}$)^{31}P are taken to be 93%, 93%, 88%, 33%, 33%, 68% and 68% of the cross section for ^{28}Si(p,x$\gamma_{1.369}$)^{24}Mg, respectively, based on the measurements at $\sim$140 MeV by Foley et al. (1962a). (The NaI detector measurements of Foley et al. (1962a) did not resolve the doublets 1.249 & 1.266, 2.029 & 2.034 and 2.232 & 2.234 MeV and we assume equal cross section for each line of the doublet.)

We have included the 3.736 MeV line (Table 5) produced by inelastic interactions of

protons and α particles with ^{40}Ca. The cross section for the reaction ^{40}Ca(p,p$'\gamma_{3.736}$)^{40}Ca was taken to be 1.5 times the cross section for ^{28}Si(p,p$'\gamma_{1.779}$)^{28}Si as determined by RKL using the recoil method. Similarly, the cross section for the reaction ^{40}Ca($\alpha, \alpha'\gamma_{3.736}$)^{40}Ca was taken to be 1.5 times the cross section for ^{28}Si($\alpha, \alpha'\gamma_{1.779}$)^{28}Si.

2.9. Lines from Reactions of Fe

The strongest lines produced by inelastic reactions on ^{56}Fe are at 0.847, 1.238 and 1.811 MeV. The cross sections for the production of these three lines were measured by the gamma-ray method on pure ^{56}Fe from ∼5 to 23 MeV by Dyer et al. (1981). The first two lines were measured from 30 to 50 MeV by Lesko et al. (1988) on natural Fe but they renormalized their results to those of Dyer et al. (1981) at ∼20 MeV. At 100 MeV, we corrected the measurements of Chang et al. (1974) for these two lines by a factor of ∼3 as established by Sadler et al. (1977). The cross sections for these two lines based on these measurements are shown in Figure 17. The cross section for the reaction ^{56}Fe(p,p$'\gamma_{1.811}$)^{56}Fe from 5 to 23 MeV is from Dyer et al. (1981). At 100 MeV, we used the Chang et al. (1974) measurement corrected as above. The cross section is also shown in Figure 17. The flattening around 30-50 MeV in all these cross sections, particularly for the 0.847 MeV line, is probably due to contributions from the spallation reaction ^{57}Fe(p,pn)^{56}Fe since the cross sections for such reactions are typically large and peak in this range.

The cross sections for the reactions ^{56}Fe(p,p$'\gamma_{1.772}$)^{56}Fe, ^{56}Fe(p,p$'\gamma_{2.094}$)^{56}Fe and ^{56}Fe(p,p$'\gamma_{2.113}$)^{56}Fe are assumed to be 14%, 12% and 10% of the cross section for ^{56}Fe(p,p$'\gamma_{0.847}$)^{56}Fe, respectively, as in RKL.

The cross section for the reaction ^{56}Fe(α,$\alpha'\gamma_{0.847}$)^{56}Fe from 2 to 6.5 MeV nucleon^{-1} was measured with the gamma-ray method on natural Fe by Seamster et al. (1984). We assume the usual inelastic behavior at higher energies. The cross section for the reaction ^{56}Fe(α,$\alpha'\gamma_{1.238}$)^{56}Fe from 3 to 6.5 MeV nucleon^{-1} was also measured by Seamster et al. (1984) and at higher energies we again assume the usual inelastic behavior. The cross sections are shown in Figure 18, where we increased the measured data by a factor of 1.09, the ratio of natural Fe to pure ^{56}Fe (Firestone & Shirley 1996).

Spallation of Fe produces a rich spectrum of lines (e.g, see Chang et al. (1974)). The strongest of these lines are at 0.931, 1.130, 1.223, 1.317, 1.408, and ∼1.435 MeV as shown in the Tables. The cross section for the reaction ^{56}Fe(p,x$\gamma_{0.931}$)^{55}Fe from 15 to 23 MeV is from Dyer et al. (1981). In the range from 30 to 50 MeV, it is from Lesko et al. (1988). At 100 MeV, we used the measurement of Chang et al. (1974), corrected by a

factor of 3 as established by Sadler et al. (1977). This cross section is shown in Figure 19. The feature at ∼1.435 MeV is composed of two lines from the reactions ^{56}Fe(p,x$\gamma_{1.434}$)^{52}Cr and ^{56}Fe(p,x$\gamma_{1.441}$)^{53}Mn. The cross section is based on the measurements by Lesko et al. (1988) at energies less than 50 MeV, and on the corrected measurement by Chang et al. (1974) at 100 MeV. The low-energy shoulder seen in the cross section is due to the (p,α) reaction producing ^{53}Mn because of the very low threshold of such a reaction. The cross section is shown in Figure 19. The cross sections for the reactions ^{56}Fe(p,x$\gamma_{1.130}$)^{54}Fe and ^{56}Fe(p,x$\gamma_{1.223}$)^{55}Fe and the combined cross section for the reactions ^{56}Fe(p,x$\gamma_{1.408}$)^{55}Fe and ^{56}Fe(p,x$\gamma_{1.408}$)^{54}Fe are from Lesko et al. (1988) at energies less than 50 MeV and from the corrected Chang et al. (1974) measurement at 100 MeV. The low-energy shoulder in the last cross section is probably due to the reaction of the isotope ^{54}Fe(p,p$'\gamma_{1.408}$)^{54}Fe in the natural target of Lesko et al. (1988). These three cross sections are shown in Figure 20. The cross section for the reaction ^{56}Fe(p,pn$\gamma_{1.317}$)^{55}Fe was taken to be 65% of the cross section for ^{56}Fe(p,pn$\gamma_{0.931}$)^{55}Fe, based on the measurements of Dyer et al. (1981) and Lesko et al. (1988).

The cross section for the reaction ^{56}Fe(p,n$\gamma_{0.812}$)^{56}Co was measured by Dyer et al. (1981) from 7 to 23 MeV. The ratio of this cross section to that of the total ^{56}Fe(p,n)^{56}Co reaction is approximately energy independent at a value of ∼24%. The presence of this line implies an additional line at 0.158 MeV whose intensity is at least equal to that of 0.812 MeV line. We take its cross section to be equal to that of the 0.812 MeV line. The cross section for the total ^{56}Fe(p,n)^{56}Co reaction, also measured by Dyer et al. (1981), is given in Figure 19.

Chang et al. (1974) measured several other Fe spallation lines. We include here those lines whose cross sections at 100 MeV are at least 10% of that of the strongest line, that at ∼1.435 MeV. These are lines at 0.092, 0.411, 0.477, 0.744, 0.984, 1.312, 1.334 and 1.370 MeV and their cross sections are taken to be 15%, 19%, 14%, 23%, 13%, 30%, 13% and 13% of the cross section for producing the 1.435 MeV line based on the measurements of Chang et al. (1974). (The Chang et al. (1974) relative cross sections are in good agreement with Sadler et al. (1977).)

The heavy element Fe has many new channels of reactions with α particles. Strong lines are produced by the reactions (α,n), (α,2n), (α,p) and (α,pn). The (α,n) reaction produces a rich spectrum of gamma-ray lines from ^{59}Ni. The strongest line is at 0.339 MeV. Seamster et al. (1984) have measured the cross section for this reaction at 4 and 6 MeV nucleon^{-1}. Seamster et al. (1984) have also measured the cross sections for the reactions ^{56}Fe(α,pn$\gamma_{1.049}$)^{58}Co (measured between 4.75 and 6.5 MeV nucleon^{-1}) and ^{56}Fe(α,n$\gamma_{1.428}$)^{59}Ni (measured between 4.75 and 6 MeV nucleon^{-1}). These cross sections, shown in Figure 21, were constructed using these measurements and the usual behavior near threshold and at

high energies. Seamster et al. (1984) have also measured the cross sections for the following unresolved line pairs (1) ^{56}Fe(α,n$\gamma_{0.999}$)^{59}Ni and ^{56}Fe(α,2n$\gamma_{1.005}$)^{58}Ni (measured between 2 and 6.5 MeV nucleon^{-1}), (2) ^{56}Fe(α,n$\gamma_{1.189}$)^{59}Ni and ^{56}Fe(α,p$\gamma_{1.190}$)^{59}Co (measured between 2.25 and 6.5 MeV nucleon^{-1}) and (3) ^{56}Fe(α,p$\gamma_{1.460}$)^{59}Co and ^{56}Fe(α,2n$\gamma_{1.454}$)^{58}Ni (measured between 3 and 6.5 MeV nucleon^{-1}). We use these measurements together with the usual behavior near threshold and at high energies to construct the cross sections shown in Figure 22. For the three doublets mentioned above, we use average line energies of 1.002, 1.189 and 1.456 MeV, respectively. Based on the Seamster measurements, we take the cross section for the reaction ^{56}Fe(α,n$\gamma_{1.367}$)^{59}Ni to be equal to the cross section for the doublet at ∼1.189 MeV. All of the lines discussed in this paragraph are from Co and Ni which are heavier than ^{56}Fe. These elements are not significantly abundant in the solar atmosphere and can only be produced by α reactions on ^{56}Fe and not from proton spallation of heavier targets. Therefore, they provide a valuable diagnostic of the accelerated α particles. This was suggested and explored by Mandzhavidze et al. (1999).

2.10. Long Duration Gamma-Ray Line Emission from Radionuclei

Very long duration gamma-ray line emission is expected from deexcitations of nuclei resulting from the decay of long lived radionuclei that are themselves produced by the accelerated particles. Such lines can be very useful because the nuclei are stopped by energy losses in the solar atmosphere before they decay and the lines are therefore very narrow. The long lifetimes also mean the interaction site may be detectable for weeks after the flare. Such long duration very narrow lines from flare-produced radioactivity have not yet been observed. Their detection, hopefully with HESSI, could measure the size and development of the radioactive patch and would provide unique information on mixing and transport processes in the solar atmosphere. The most promising such line is at 0.847 MeV resulting from ^{56}Co decay into ^{56}Fe with a mean life of 111.5 days (Ramaty & Mandzhavidze 2000a). The ^{56}Co is produced in (p,n) reactions of both accelerated protons with ambient Fe and accelerated Fe with ambient H. The (p,n) cross section was measured by Dyer et al. (1981) as discussed above and is shown in Figure 19. The 0.847 MeV line is accompanied by additional lines, also resulting from ^{56}Co decay to ^{56}Fe, at 1.038, 1.238, 1.771 and 2.598 MeV with cross sections of 14%, 68%, 16% and 17% relative to that of the 0.847 MeV line. The decay of ^{55}Co to ^{55}Fe produces lines at 0.477, 0.931 and 1.408 MeV with cross sections of 27%, 100% and 23% relative to that of the ^{56}Fe(p,x)^{55}Co reaction. The decay of ^{54}Mn to ^{54}Cr produces a line at 0.835 MeV with a cross section equal to that of the ^{56}Fe(p,x)^{54}Mn reaction. The decay of ^{52}Mn to ^{52}Cr produces lines at 0.744, 0.936 and 1.434 MeV with cross sections of 91%, 95% and 100% relative to that of the ^{56}Fe(p,x)^{52}Mn reaction. The above

branching ratios have been taken from (Firestone & Shirley 1996) and the cross sections for the ^{56}Fe(p,x)^{55}Co, ^{56}Fe(p,x)^{54}Mn and ^{56}Fe(p,x)^{52}Mn reactions were given by RKL (their Figure 12).

The prompt line at 0.478 MeV produced by the reaction ^{4}He(α,p)^{7}Li* as discussed in §2.1 can also be produced by the reaction ^{4}He(α,n)^{7}Be(ϵ)^{7}Li*(10.5%) with a mean life of 76.9 days. The cross section for the reaction ^{4}He(α,n)^{7}Be(total) is shown in Figure 2. Although the cross section is not large, this line can be important in solar flares relative to the 0.847 MeV long duration Fe line discussed above because the ambient ^{4}He/^{56}Fe ratio could be as high as 1000 and the abundance of accelerated ^{4}He can be significantly enhanced.

3. Discussion

We have studied excitation functions for production of gamma-ray lines following energetic proton and α reactions with the abundant constituents of cosmic matter. We have presented the cross sections for proton and α reactions with He, C, N, O, Ne, Mg, Al, Si, S, Ca and Fe. These cross sections are also applicable to the inverse reactions, where energetic particles heavier than He interact with ambient H and He, by way of a kinematic transformation.

The most important range of accelerated particle energies for gamma-ray line production is from $\sim$1 to a few tens of MeV nucleon^{-1} because most cross sections typically peak in this range and because accelerated particle energy spectra (particularly solar flares) are steep. Fortunately, this range is well covered by good laboratory measurements, especially for the strongest gamma-ray lines, and thus establishes solid credibility for astronomical gamma-ray line spectroscopy. From several tens to several hundred MeV nucleon^{-1}, the presented cross sections are sometimes based on general trends of asymptotic behavior for various types of reactions rather than laboratory measurements. This is particularly true for α-particle induced reactions (e.g., the important reaction ^{20}Ne(α,$\alpha'\gamma_{1.634}$)^{20}Ne is only measured up to $\sim$10 MeV nucleon^{-1}). But calculations of gamma-ray yields are not sensitive to this uncertainty when the α/proton ratio is small or when the energetic particle spectrum is steep. Nevertheless, new laboratory measurements in this range are needed, particularly for the α-particle induced reactions.

Reactions induced by energetic ^{3}He are often not important because the ^{3}He/hydrogen ratio is typically $\sim10^{-5}$. But in solar flares, ^{3}He can be significantly enhanced. There are very few laboratory measurements of gamma-ray line yields from ^{3}He-induced reactions. We have included here only the cross sections for the reactions ^{16}O(^{3}He,p)^{18}F* (producing lines

at 0.937, 1.042 and 1.081 MeV) and ^{4}He(^{3}He,p)^{6}Li* (producing a line at 3.563 MeV). A comprehensive program of laboratory measurements of gamma-ray lines from ^{3}He-induced reactions, similar to that done for proton and α-particle induced reactions, is needed.

Reuven Ramaty pioneered and passionately pursued the study of gamma-ray line spectroscopy for more than 30 years. The research reported in this paper was his last active effort. B. Kozlovsky thanks G. Share and J. Kurfess for their hospitality at the Naval Research Laboratory. The authors thank G. Share for advice, encouragement and many useful comments on the manuscript. B. Kozlovsky acknowledges the Israeli Science Foundation for support. Part of this research was supported by NASA DPR S92680F and W19977.

A. Appendix

In addition to the cross section Figures given in the present paper, we also supply numerical values for the cross sections for all lines listed in Table 1. We emphasize that meaningful use of these data requires careful study of the text and Table provided in the paper. The cross sections are available at the web site http:xxx.

There are three tables. The first two tables (A1 and A2) provide the necessary information needed to use the cross sections given in the third table (A3). Table A1 includes all prompt gamma-ray lines and lines from radioactive nuclei with mean lifetimes less than 100 s. Table A2 includes lines from radioactive nuclei with mean lifetimes greater than 100 s and less than 10^7 s. In solar flare research, these two types of lines are typically analyzed separately. The first set of lines is relevant for analysis of radiation produced during a flare. The second set is relevant for analysis of radiation extending beyond the flare itself. In these two tables, the first column is the line energy in MeV and the second column is the target nucleus of the reaction giving rise to the line. This nucleus is not necessarily the nucleus producing the line emission; this information can be obtained from Table 1 in the paper. For example, the 4.44 MeV line from carbon can be produced through inelastic reactions with carbon as the target and also through spallation reactions with nitrogen and oxygen as the targets. The third column is the name of the cross section for proton-induced reactions. This name identifies the cross section that is given in the third table (A3). The fourth column gives the multiplicative factor which must be applied to all values of that cross section. As explained in the paper, for some lines we approximate the cross section for which complete laboratory data are not available by using the cross section for a similar reaction for which complete data are available but scaled with the multiplicative factor. Therefore, several lines can be related to one cross section. Columns five and six give the same information as

columns three and four but for alpha-induced reactions. Columns seven and eight give the same information but for 3He-induced reactions.

We note that Tables A1 and A2 do not include cross sections for every combination of projectile and target for every line (as indicated by the letter n in the Table). There are two possible reasons for this. The first is that the given line cannot be produced by that combination; e.g., the 0.429 MeV line from 7Be can only be produced by alpha interaction with a 4He target. The second is that reliable laboratory measurements for that combination are not available and so we ignore it if that line is expected to be weak. This is discussed in Section 3 of the paper.

Table three contains the cross section values for all of the reactions. The first column gives the name of the cross section as identified in Tables A1 and A2. The second column gives the number of energies for which cross section values are given. The third column gives the energy values (in MeV nucleon^{-1}) and the fourth column gives the cross section value (in milliBarn).

The cross sections in the code will be continuously modified as the result of new laboratory measurements and these updated versions will be available at the web site

http://lheawww.gsfc.nasa.gov/users/ramaty/ViewPubs/ramaty.html.

REFERENCES

Alard, J. P. et al. 1974, Nuovo Cimento (Letters), 10, 841

Chang, C. C., Wall, N. S., and Fraenkel, Z. 1974, Phys. Rev. Letters, 33, 1493

Chupp, E. L. 1984, Ann. Rev. Astron. Astrophys., 22, 359

Clegg, A. B., Foley, K. J., Salmon, G. L. & Segal, R. E. 1961, Proc. Phys. Soc., 78, 681

Dyer, P., Bodansky, D., Seamster, A. G., Norman, E. B. & Maxson, D. R. 1981, Phys. Rev., C23, 1865

Dyer, P., Bodansky, D., Leach, D. D., Norman, E. B. & Seamster, A. G. 1985, Phys. Rev., C32, 1873

Feldman, U. 1992, Phys. Scr., 46, 202

Firestone, R. B. & Shirley, V. S, Table of Isotopes, 1996 (New York: Wiley)

Foley, K. J., Clegg, A. B. & Salmon, G. L. 1962, Nucl. Phys., 37, 23

Foley, K. J., Salmon, G. L. & Clegg, A. B. 1962, Nucl. Phys., 31, 43

Geiss, J. 1998, Space Sci. Rev., 85, 241

Goryachev, Y. M., Kanavets, V. P., Kirpichnikov, I. V., Levintov, I. I., Morozov, B. V., Nikiforov, N. & Starostin, A. S. 1973, Sov. J. Nucl. Phys., 17, 476

Hahn, R. L. & Ricci, E. 1966, Phys. Rev., 146, 650

Harrison, W. D. 1967, Nucl. Phys., A92, 260

Halbert, M. L., van der Woude, A., & O'Fallon, N. M. 1973, Phys. Rev., C8, 1621

Heggie, J. C. P., Switkowski, Z. E., & Clark, G. J. 1980, Nuclear Instruments and Methods, 168, 125

Janus, R. Y. & McCarthy, I. E. 1974, Phys. Rev., C10, 1041

Kiener, J. et al. 1998, Phys. Rev., C58, 2174

King, C. H., Austin, S. M., Rossner, H. H., & Chien, W. S. 1977, Phys. Rev. C16, 1712

Koepke, J. A., & Brown, R. E. 1977, Phys. Rev. C16, 18

Kozlovsky, B., & Ramaty, R. 1974, ApJ, 191, L43

Lang, F. L., Werntz, C. W., Crannell, C. J., Trombka, J. I. & Chang, C. C. 1987, Phys. Rev., C35, 1214

Leikov, N. G. et al. 1993, A&A Suppl., 97, 345

Lesko, K. T. et al. 1988, Phys. Rev., C37, 1808

Mandzhavidze, N., Ramaty, R., & Kozlovsky, B. 1997, ApJ, 489, L99

Mandzhavidze, N., Ramaty, R., & Kozlovsky, B. 1999, ApJ, 518, 918

Mercer, D. J. et al. 2001, Phys Rev. C, to be published

Mercer, D. J., Austin, S. M. & Glagola, B. G. 1997, Phys. Rev. C55, 946

Murphy, R.J., Ramaty, R., Kozlovsky, B., & Reames, D.V. 1991, ApJ, 371, 793

Murphy, R.J., Share, G. H., Grove, J. E., Johnson, W. N., Kinzer, R. L., Kurfess, J. D., Strickman, M. S., & Jung, G. V. 1997, ApJ, 490, 883

Narayanaswarmy, J., Dyer, P., Faber, S. R. & Austin, S. M. 1981, Phys. Rev., C24, 2727

Ramaty, R., Kozlovsky, B. & Lingenfelter, R. E. 1979, ApJS, 40, 487

Ramaty, R., Mandzhavidze N., Kozlovsky, B., & Murphy, R.J. 1995, ApJ, 445, L193

Ramaty, R., Mandzhavidze N., & Kozlovsky, B. 1996, in: High Energy Solar Physics, eds. R. Ramaty, N. Mandzhavidze, & X.-M. Hua, AIP Conf. Proc. 374, (New York, AIP), 172

Ramaty, R., & Mandzhavidze N. 2000, in Highly Energetic Physical Processes and Mechanisms for Emission from Astrophysical Plasmas, eds. P. C. H. Martens, S. Tsuruta and M. A. Weber, IAU Symp. 195, ASP, 123

Ramaty, R., Tatischeff, V., Kozlovsky, B., & Mandzhavidze N. 1996, ApJ534, L207

Reames, D. V. 1998, Space Sci. Rev., 85, 327

Sadler, M., *et al.*, 1977, *Phys. Rev. Letters*, **38**, 950.

Schrank, G., Warburton, E. K. & Daehnick, W. W. 1962, Phys. Rev., 127, 2159

Seamster, A. G., Norman, E. B., Leach, D. D., Bodansky, D. 1984, *Phys. Rev.* C29, 394

Seidlitz, L., Bleuler, E. & Tendam, D. J. 1958, Phys. Rev., 110, 682

Share, G. H., & Murphy, R.J. 1995, ApJ, 452, 933

Share, G. H., & Murphy, R.J. 1997, ApJ, 485, 409

Share, G. H., Murphy, R.J., & Ryan, J. 1997, in: Proceedings of the Fourth Compton Symposium, AIP Conf. Proc., 410, 17

Share, G. H., & Murphy, R. J. 1998, ApJ, 508, 876

Slobodrian, R. J., & Conzett H. E. 1982, Zeitschrift fur Physik A, 308, 15

Tatischeff, V., Cassé, M., Kiener, J., Thibaud, J.-P. & Vangioni-Flam, E. 1996, ApJ, 472, 205

Trottet, G. et al. 1996, in: High Energy Solar Physics, eds. R. Ramaty, N. Mandzhavidze & X.-M. Hua, AIP Conf. Proc. 435, (AIP: New York), 153

Yoshimori, M. 1990, ApJS, 73, 227

Yoshimori, M., Suga, K., Morimoto, K., Hiraoka, T., Sato, J., Kawabata, K & Ohki, K. 1994, ApJS, 90, 639

Zobel, W., Maienschien, F. C., Todd, J. H. & Chapman, G. T. 1968, Nucl. Sci. Eng., 32, 392

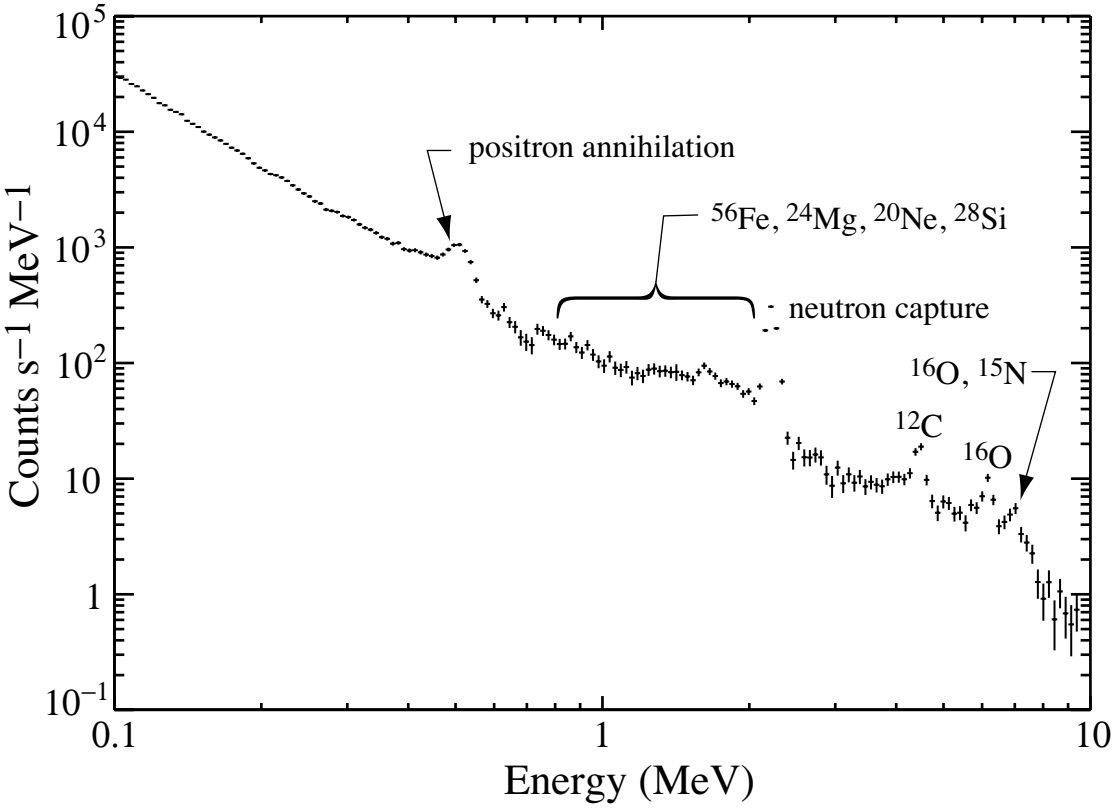

Fig. 1.— Gamma-ray count spectrum from the 1991 June 4 solar flare observed by *CGRO*/OSSE (Murphy et al. 1997). The sources of some of the line features are indicated.

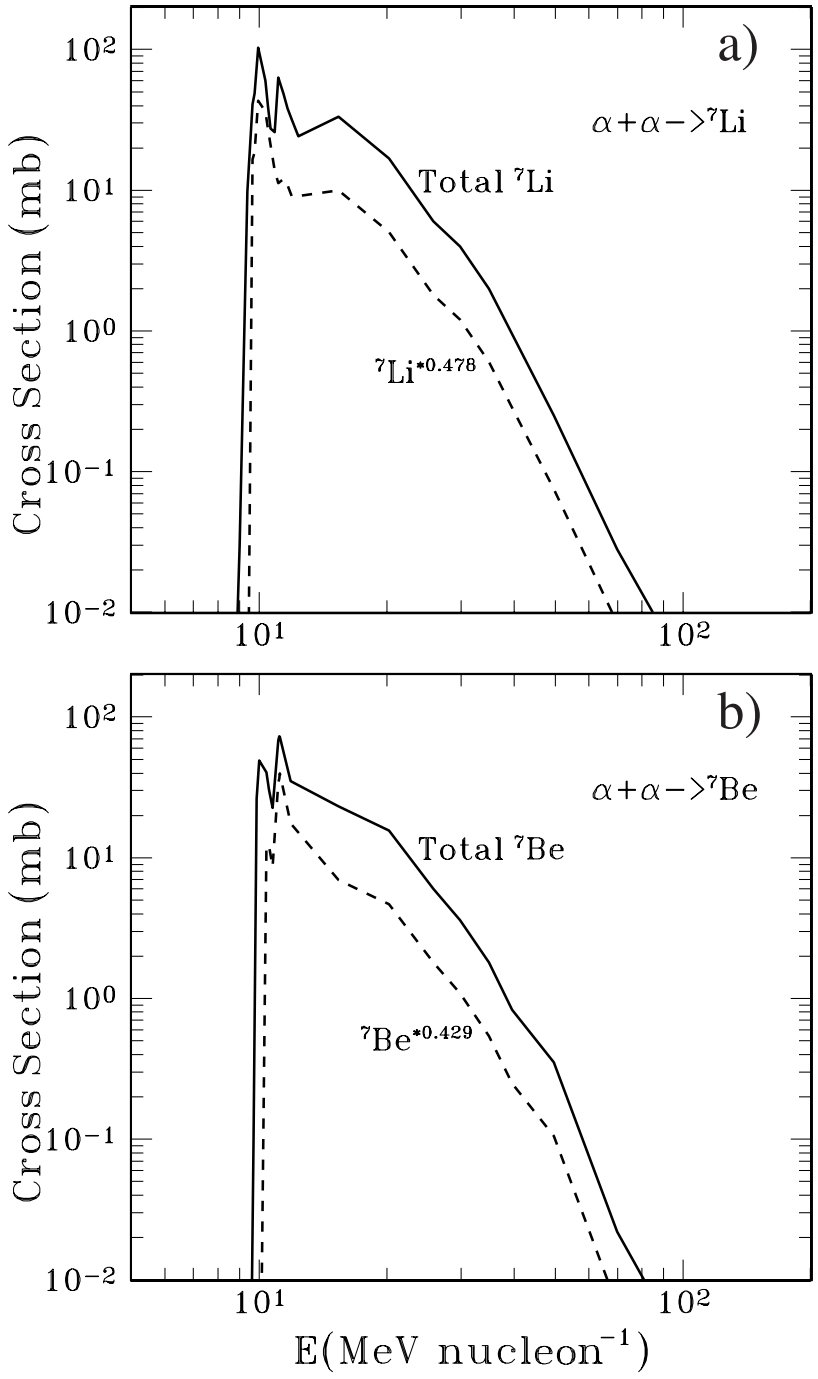

Fig. 2.— Cross sections for α reactions with ^{4}He producing ^{7}Li and ^{7}Be. In panel a), the solid curve is for total (ground + excited state) production and the dashed curve is for ^{7}Li$^{*0.478}$ production. Panel b) shows the corresponding cross sections for production of total ^{7}Be and ^{7}Be$^{*0.429}$.

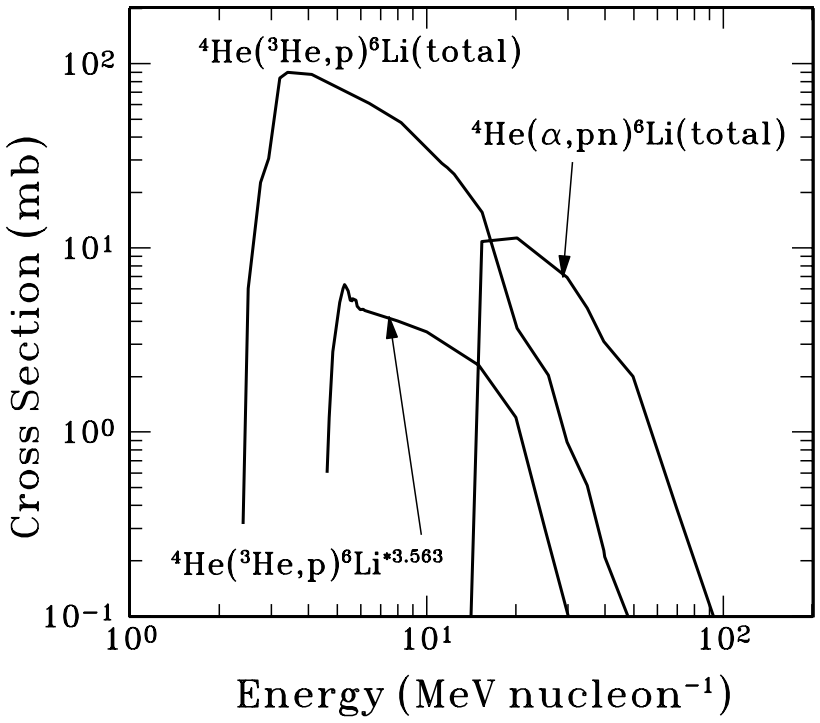

Fig. 3.— Cross sections for ^{3}He and α reactions with ^{4}He to produce total ^{6}Li and ^{6}Li$^{*3.563}$.

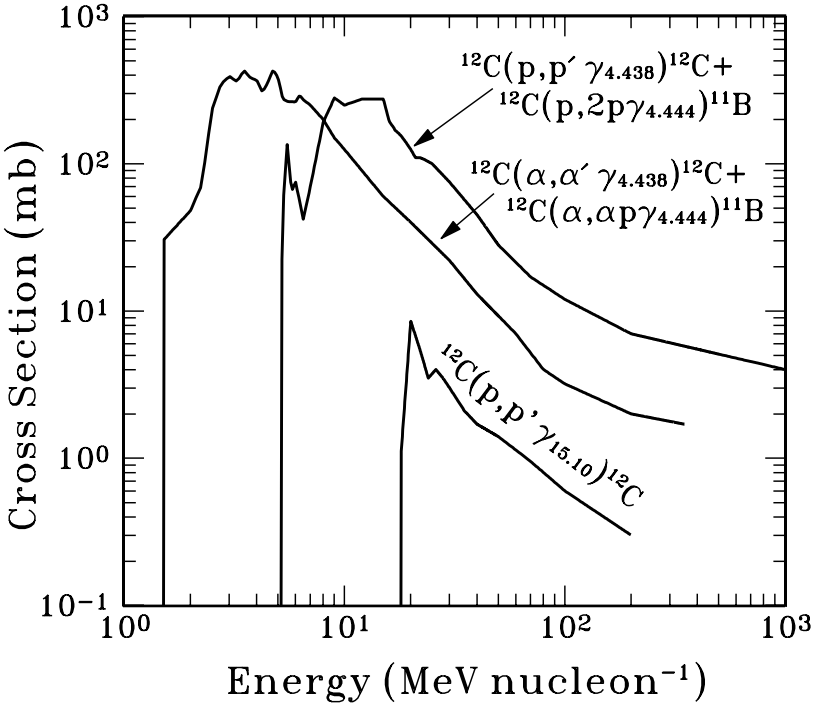

Fig. 4.— Cross sections for production of the 4.44 and 15.1 MeV lines from proton and α reactions with ^{12}C.

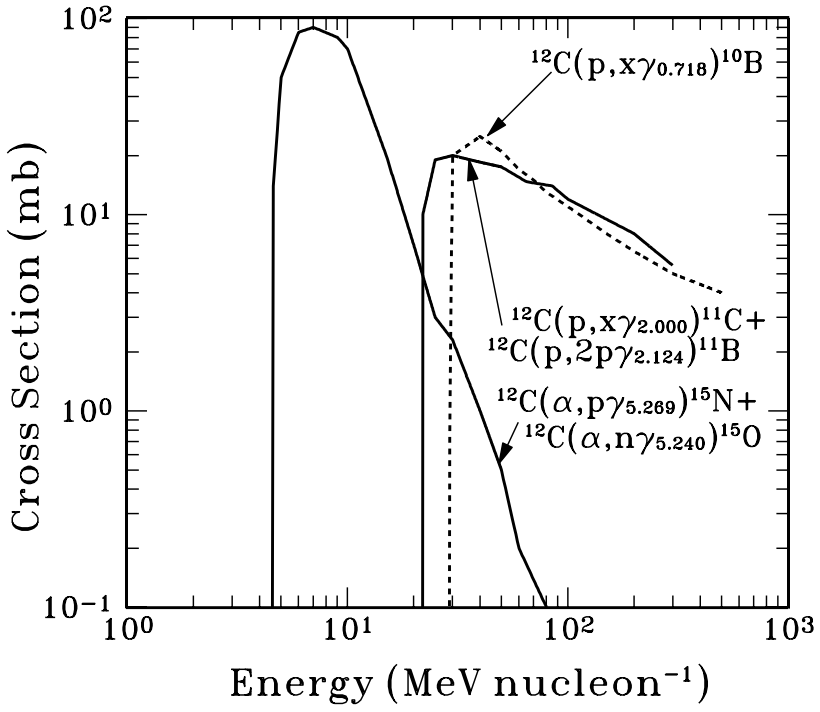

Fig. 5.— Cross sections for the production of the 0.718 MeV line of ^{10}B, the (2.000 + 2.124) MeV lines of ^{11}C and ^{11}B, and the (5.269 + 5.240) MeV lines of ^{15}N and ^{15}O from proton and α reactions with ^{12}C.

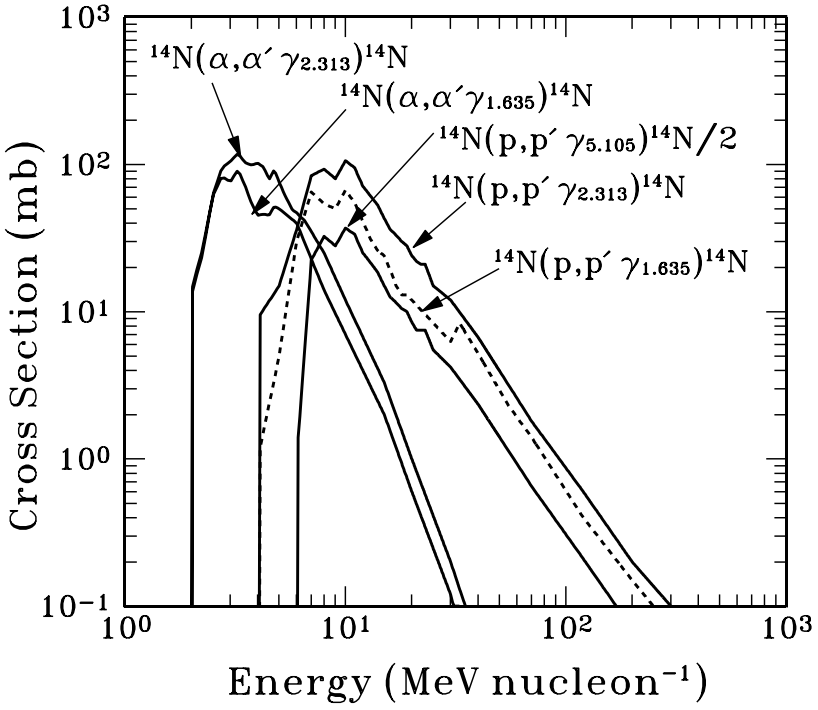

Fig. 6.— Cross sections for production of the 1.635, 2.313 and 5.105 MeV lines from proton and α reactions with ^{14}N. The cross section for the 5.105 MeV line has been divided by 2 for clarity.

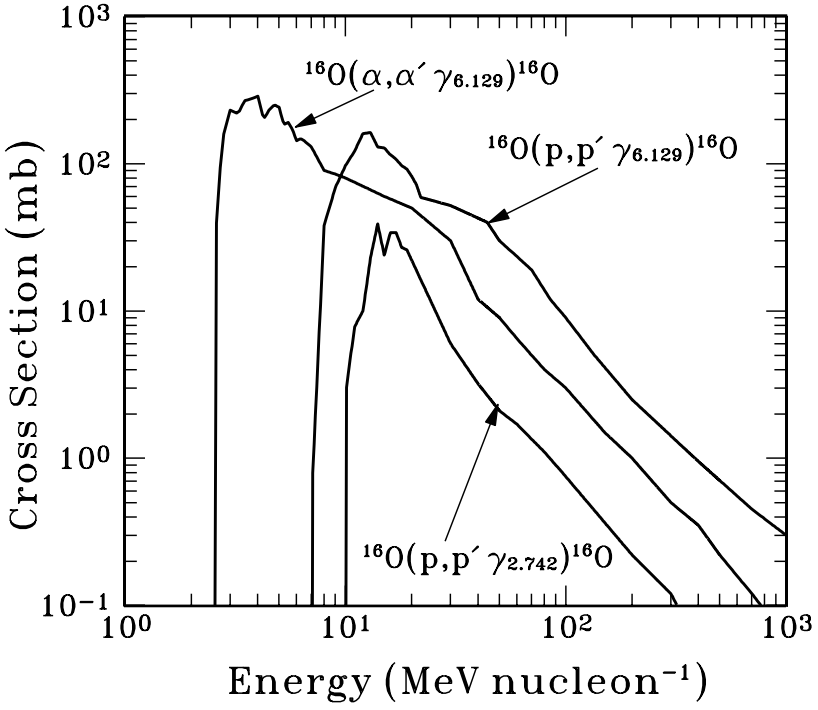

Fig. 7.— Cross sections for production of the 2.742 and 6.129 MeV lines from proton and α reactions with ^{16}O.

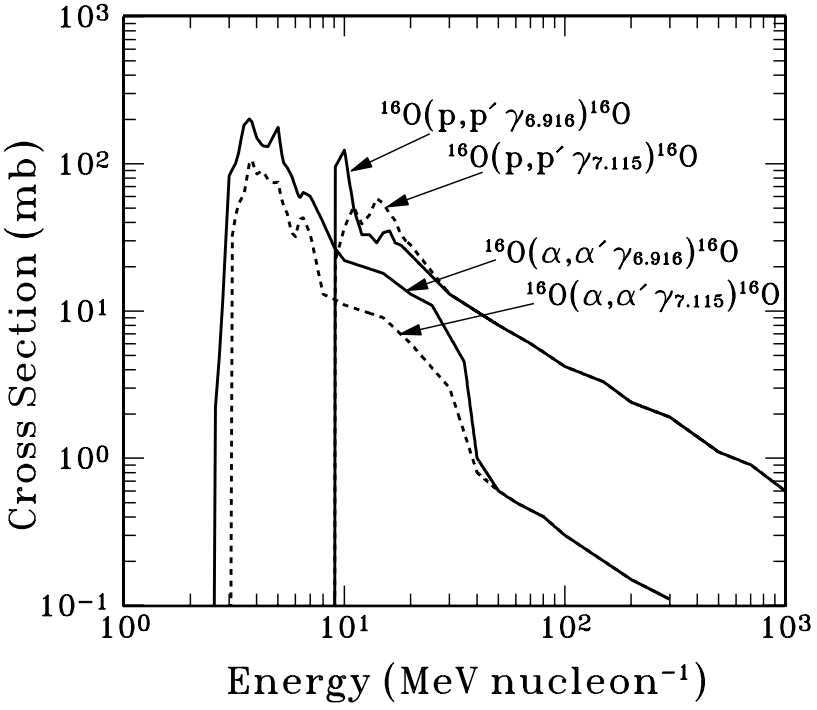

Fig. 8.— Cross sections for production of the 6.916 and 7.115 MeV lines from proton and α reactions with ^{16}O.

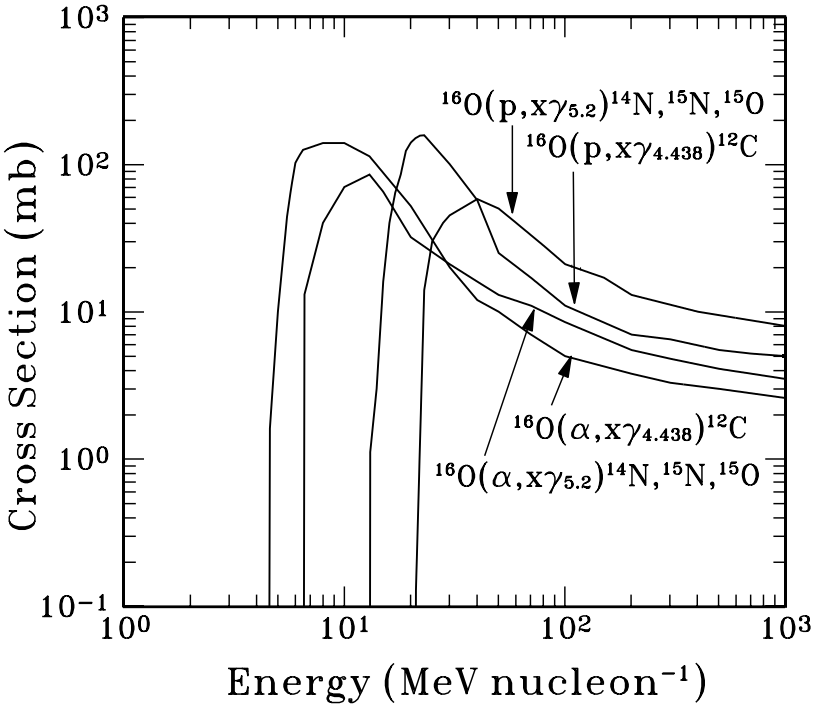

Fig. 9.— Cross sections for production of the 4.438 and ∼5.2 MeV lines from proton and α spallation reactions with ^{16}O.

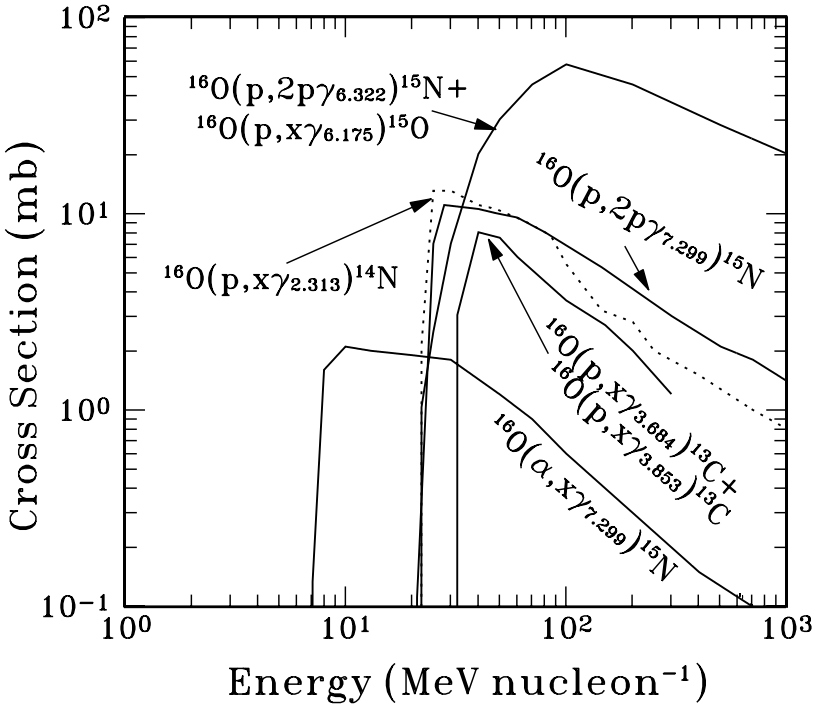

Fig. 10.— Cross sections for production of the 2.313, ∼3.7, ∼6.2 and 7.299 MeV lines from proton and α spallation reactions with ^{16}O.

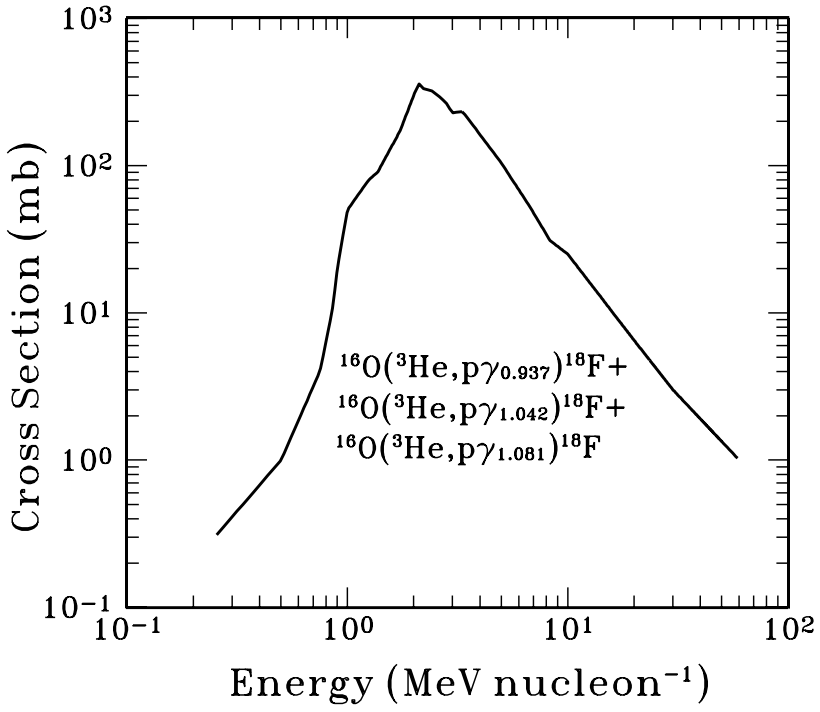

Fig. 11.— Summed cross section for the production of the 0.937, 1.042 and 1.081 MeV lines from ^{3}He reactions with ^{16}O. The assumed partial cross section for each line is discussed in the text.

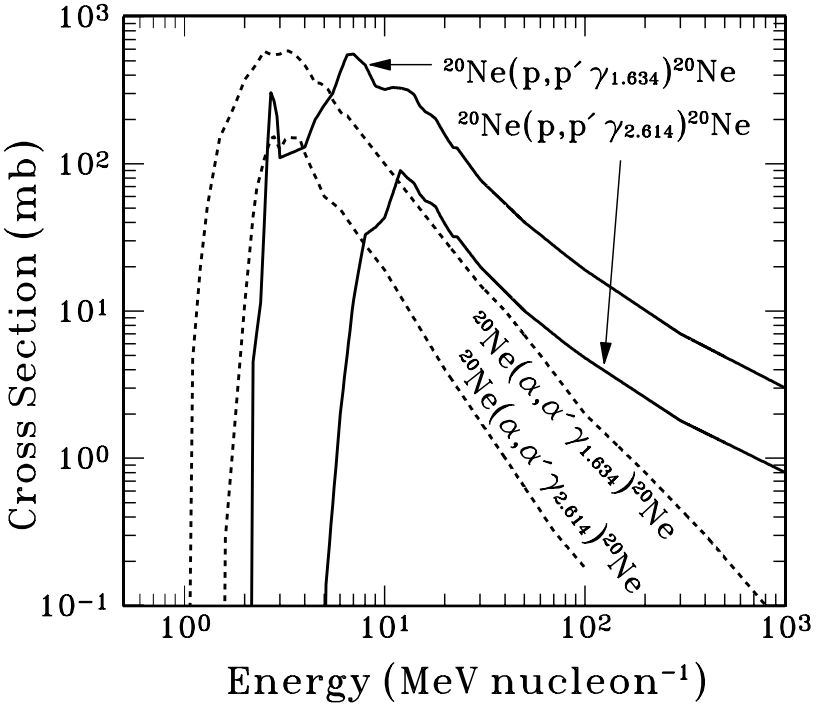

Fig. 12.— Cross sections for production of the 1.634 and 2.614 MeV lines from proton and α reactions with ^{20}Ne.

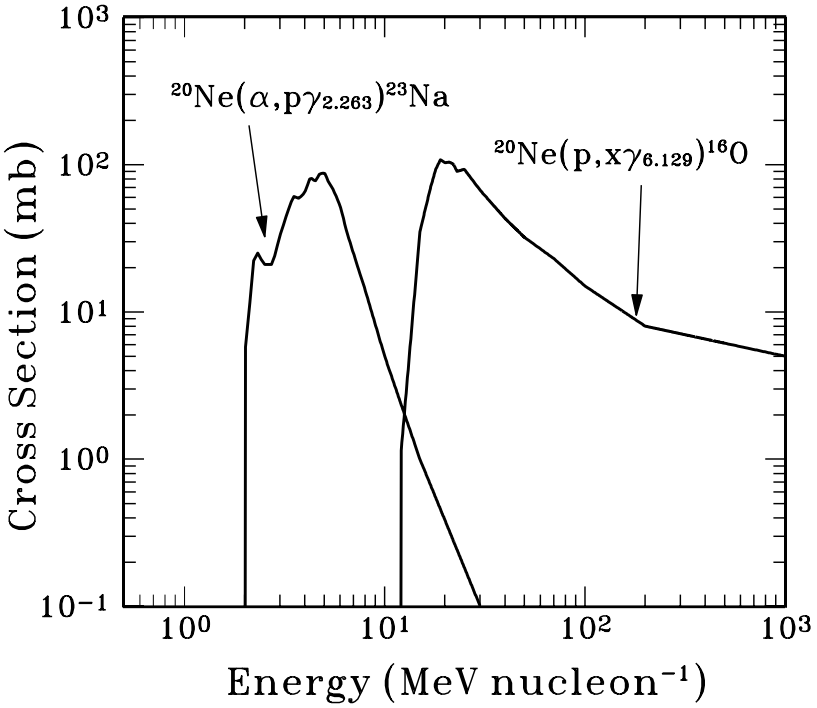

Fig. 13.— Cross sections for production of the 2.263 MeV line of ^{23}Na and the 6.129 MeV line of ^{16}O from proton and α reactions with ^{20}Ne.

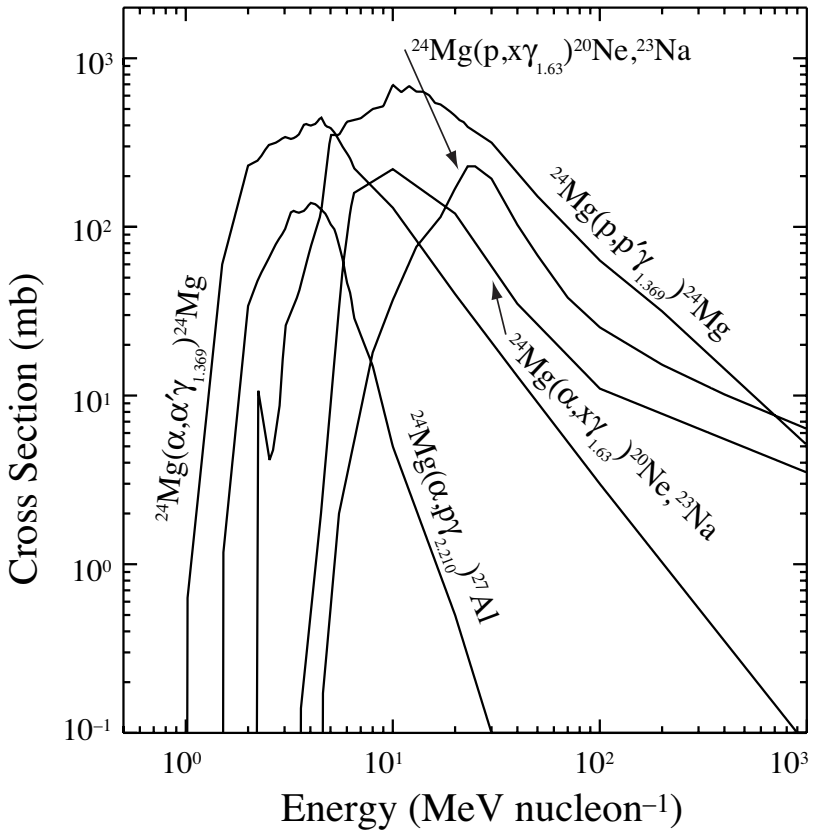

Fig. 14.— Cross sections for production of the 1.369 MeV line of ^{24}Mg, the (1.634 + 1.636) MeV lines of ^{20}Ne and ^{23}Na and the 2.210 MeV line of ^{27}Al from proton and α reactions with ^{24}Mg.

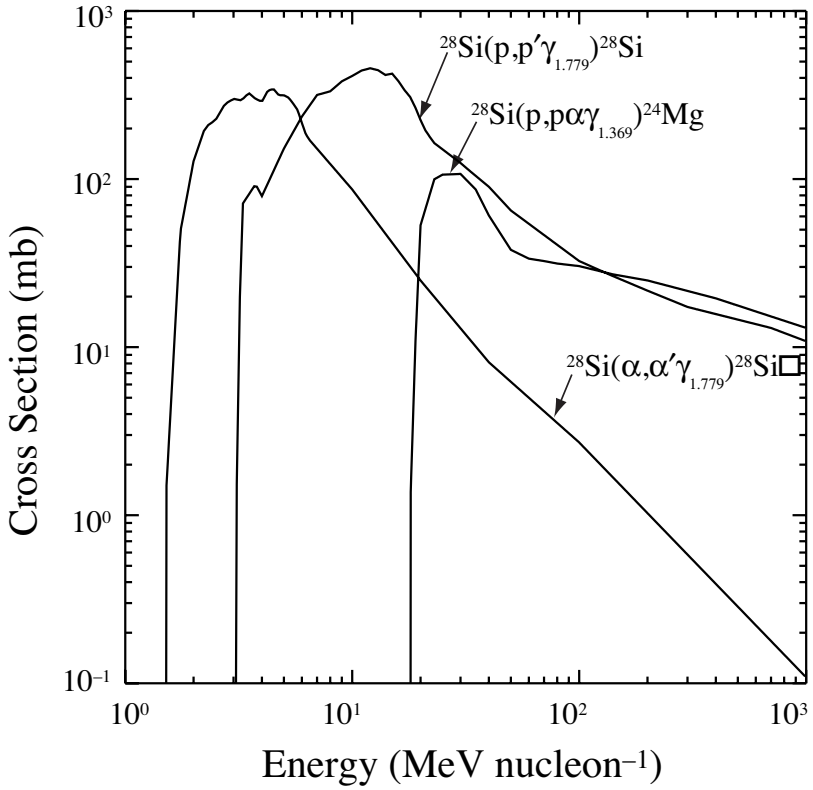

Fig. 15.— Cross sections for production of the 1.779 MeV line of ^{28}Si from proton and α reactions with ^{28}Si and the 1.369 MeV line of ^{24}Mg from proton spallation reactions with ^{28}Si.

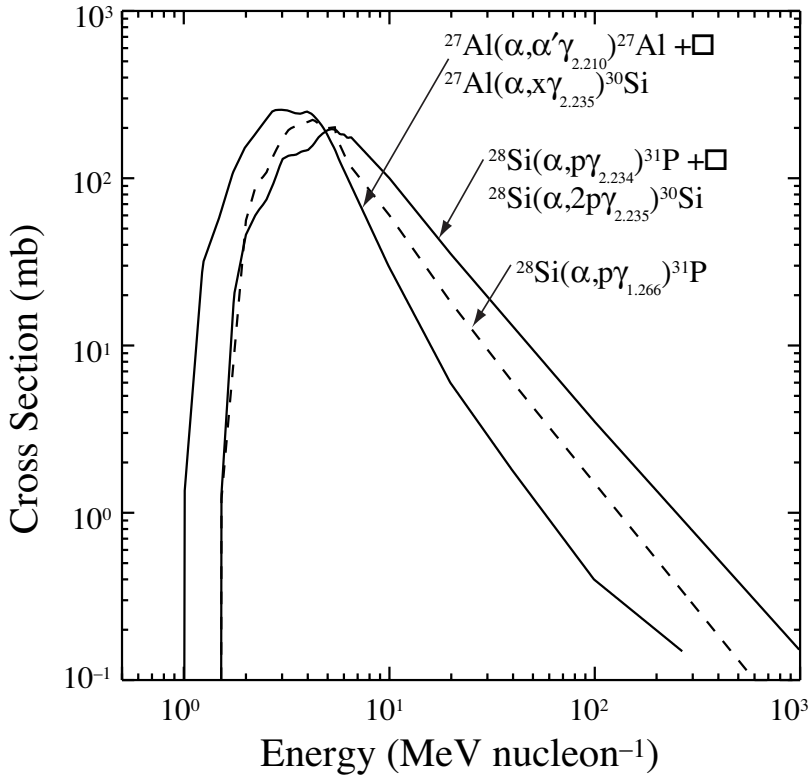

Fig. 16.— Cross sections for production of the 1.266 MeV line of ^{31}P, the (2.234 + 2.235) MeV lines of ^{31}P and ^{30}Si from α reactions with ^{28}Si and the (2.210 + 2.235) MeV lines of ^{27}Al from α reactions with ^{27}Al.

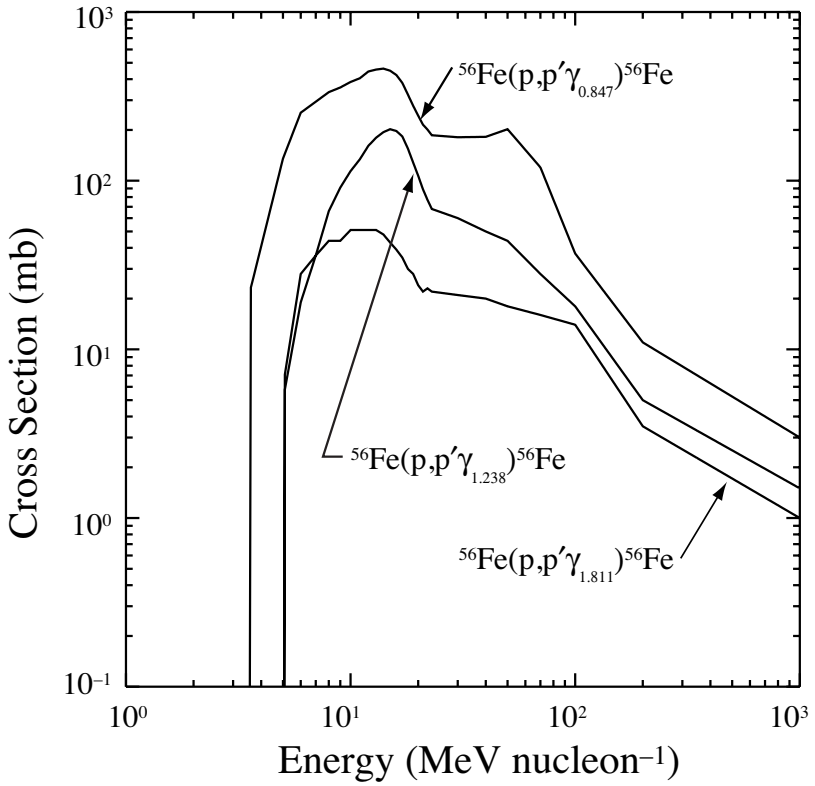

Fig. 17.— Cross sections for production of the 0.847, 1.238 and 1.811 MeV lines from proton reactions with ^{56}Fe.

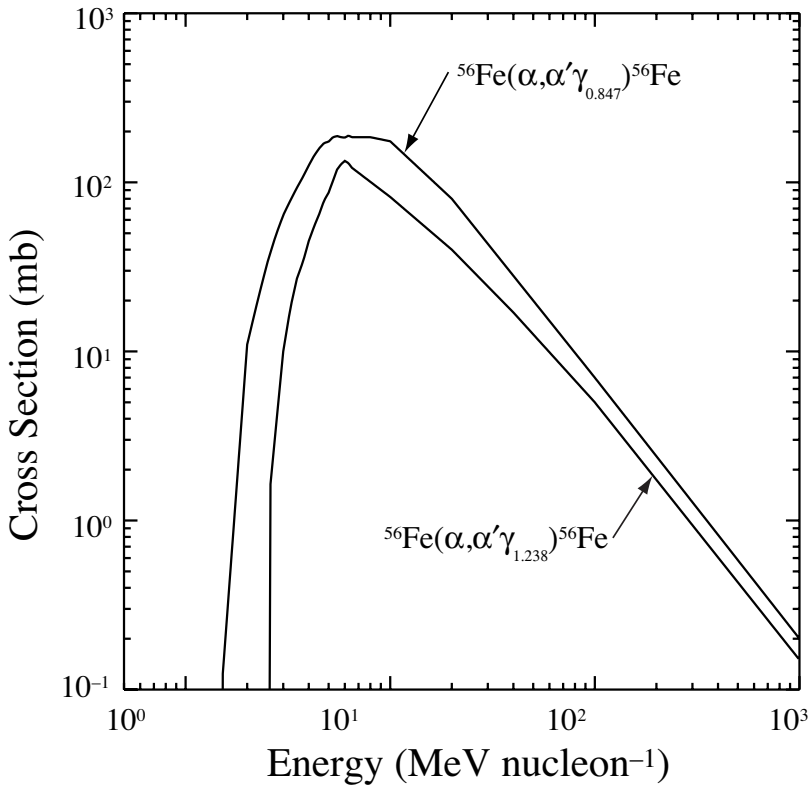

Fig. 18.— Cross sections for production of the 0.847 and 1.238 MeV lines from α reactions with ^{56}Fe.

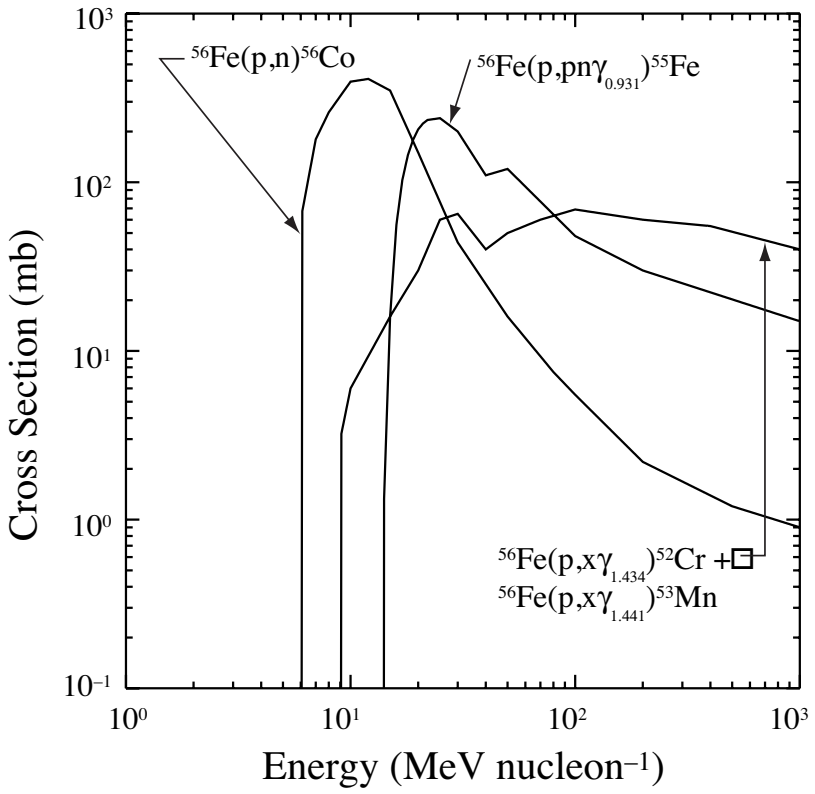

Fig. 19.— Cross sections for production of the 0.931 MeV line from ^{55}Fe and the (1.434 + 1.441) MeV lines from ^{52}Cr and ^{53}Mn from proton spallation reactions with ^{56}Fe. Also shown is the cross section for the reaction ^{56}Fe(p,n)^{56}Co.

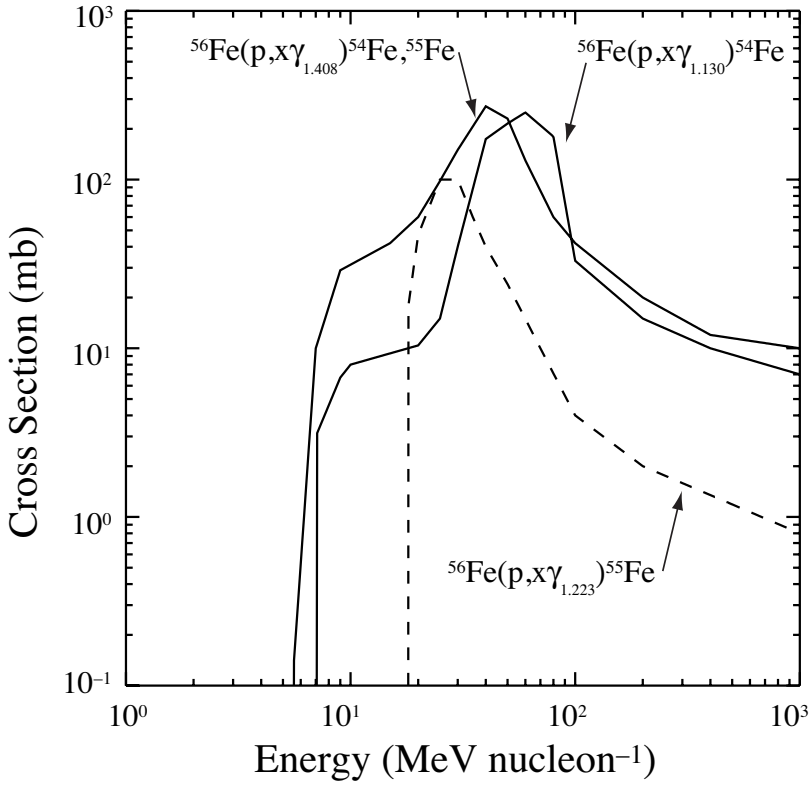

Fig. 20.— Cross sections for the production of the 1.130 MeV line of ^{54}Fe, the 1.223 MeV of ^{55}Fe and the 1.408 MeV line of ^{54}Fe and ^{55}Fe from proton spallation reactions with ^{56}Fe.

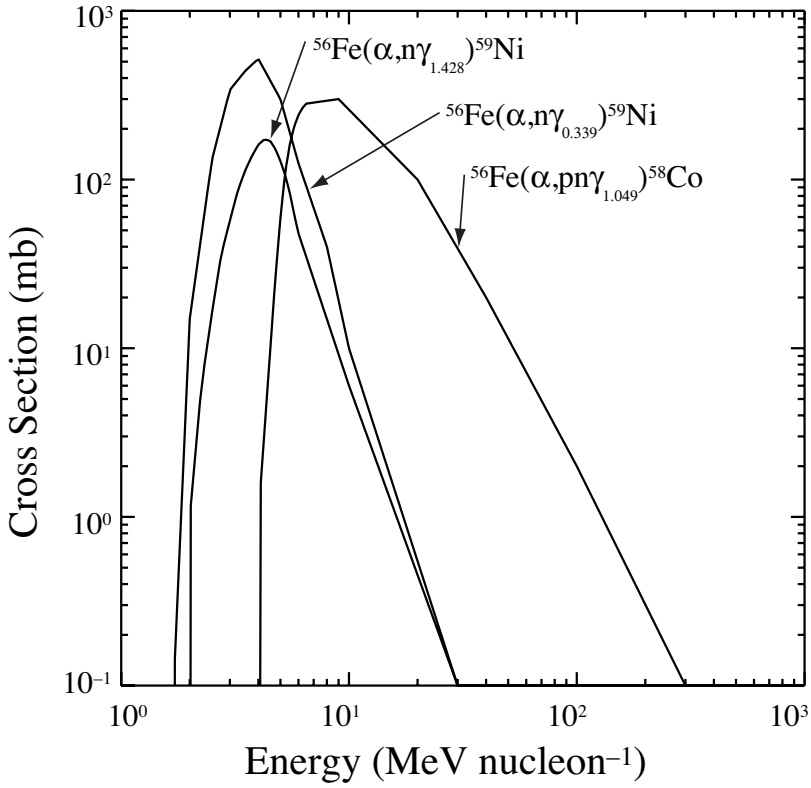

Fig. 21.— Cross sections for the production of the 0.339 MeV line of ^{59}Ni, the 1.049 MeV line of ^{58}Co and the 1.428 MeV line of ^{59}Ni from α reactions with ^{56}Fe.

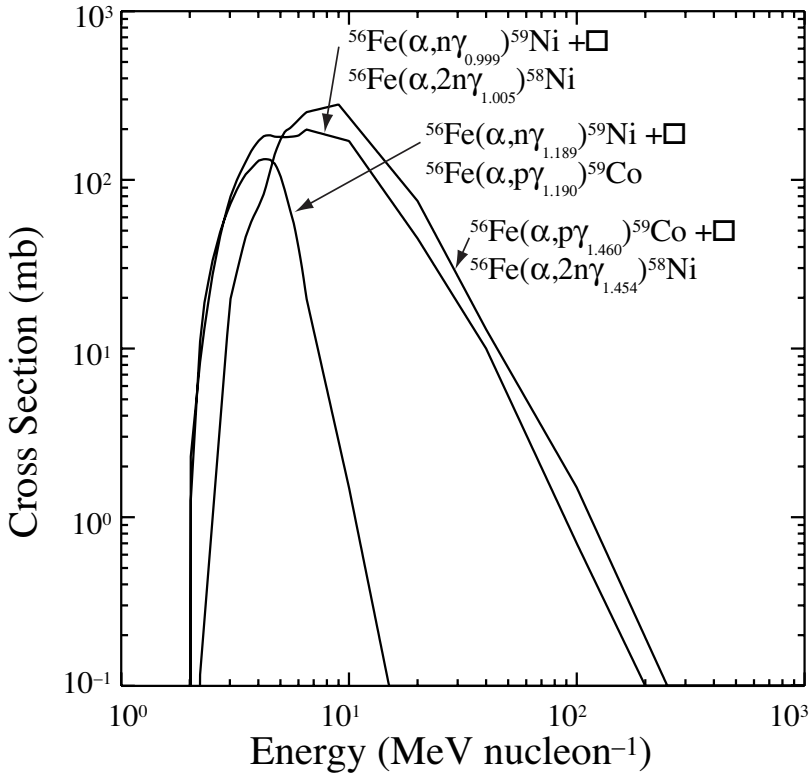

Fig. 22.— Cross sections for production of the (0.999 + 1.005) MeV lines from ^{59}Ni and ^{58}Ni, the (1.189 + 1.190) MeV lines from ^{59}Ni and ^{59}Co and the (1.460 + 1.454) MeV lines from ^{59}Co and ^{58}Ni from α reactions with ^{56}Fe.

Table 1. Gamma Ray Lines Below 1.0 MeV Ordered by Energy

Line[a]	Transition[b]	Reaction	Mean Life[c]
0.092	$^{55}Fe^{*1.408} \rightarrow ^{55}Fe^{*1.317}$	$^{56}Fe(p,x)^{55}Fe^{*}$	5.5×10^{-11}
0.110	$^{19}F^{*0.110} \rightarrow$g.s.	$^{20}Ne(p,x)^{19}F^{*}$	8.5×10^{-10}
0.158	$^{56}Co^{*0.158} \rightarrow$g.s.	$^{56}Fe(p,n)^{56}Co^{*}$	1.4×10^{-10}
0.197	$^{19}F^{*0.197} \rightarrow$g.s.	$^{20}Ne(p,x)^{19}F^{*}$	1.3×10^{-7}
0.238	$^{19}Ne^{*0.238} \rightarrow$g.s.	$^{20}Ne(p,x)^{19}Ne^{*}$	2.6×10^{-8}
0.275	$^{19}Ne^{*0.275} \rightarrow$g.s.	$^{20}Ne(p,x)^{19}Ne^{*}$	6.1×10^{-11}
0.339	$^{59}Ni^{*0.339} \rightarrow$g.s.	$^{56}Fe(\alpha,n)^{59}Ni^{*}$	9.8×10^{-11}
0.411	$^{55}Fe^{*0.411} \rightarrow$g.s.	$^{56}Fe(p,x)^{55}Fe^{*}$	8.7×10^{-12}
0.429	$^{7}Be^{*0.429} \rightarrow$g.s.	$^{4}He(\alpha,n)^{7}Be^{*}$	1.9×10^{-13}
0.440	$^{23}Na^{*0.440} \rightarrow$g.s.	$^{20}Ne(\alpha,p)^{23}Na^{*}$	1.6×10^{-12}
		$^{24}Mg(p,x)^{23}Na^{*}$	1.6×10^{-12}
0.451	$^{23}Mg^{*0.451} \rightarrow$g.s.	$^{24}Mg(p,x)^{23}Mg^{*}$	1.8×10^{-12}
0.477	$^{55}Fe^{*1.408} \rightarrow ^{55}Fe^{*0.931}$	$^{56}Fe(p,x)^{55}Fe^{*}$	5.5×10^{-11}
		$^{56}Fe(p,x)^{55}Co(e^{+},\epsilon)^{55}Fe^{*}(27\%)$	9.1×10^{4}
0.478	$^{7}Li^{*0.478} \rightarrow$g.s.	$^{4}He(\alpha,p)^{7}Li^{*}$	1.1×10^{-13}
		$^{4}He(\alpha,n)^{7}Be(\epsilon)^{7}Li^{*}(10.5\%)$	6.64×10^{6}
0.718	$^{10}B^{*0.718} \rightarrow$g.s.	$^{12}C(p,x)^{10}B^{*}$	1.0×10^{-9}
		$^{12}C(p,x)^{10}C(\epsilon)^{10}B^{*}$ (100%)	27.8
		$^{16}O(p,x)^{10}B^{*}$	1.0×10^{-9}
0.744	$^{52}Cr^{*3.114} \rightarrow ^{52}Cr^{*2.370}$	$^{56}Fe(p,x)^{52}Cr^{*}$	6.0×10^{-11}
		$^{56}Fe(p,x)^{52}Mn(e^{+},\epsilon)^{52}Cr^{*}(91\%)$	7.0×10^{5}
0.781	$^{27}Si^{*0.781} \rightarrow$g.s.	$^{28}Si(p,x)^{27}Si^{*}$	5.0×10^{-11}
0.812	$^{56}Co^{*0.970} \rightarrow ^{56}Co^{*0.158}$	$^{56}Fe(p,n)^{56}Co^{*}$	1.7×10^{-13}
0.835	$^{54}Cr^{*0.835} \rightarrow$g.s.	$^{56}Fe(p,x)^{54}Mn(e^{+},\epsilon)^{54}Cr^{*}(100\%)$	3.9×10^{7}
0.844	$^{27}Al^{*0.844} \rightarrow$g.s.	$^{28}Si(p,x)^{27}Al^{*}$	5.0×10^{-11}
0.847	$^{56}Fe^{*0.847} \rightarrow$g.s.	$^{56}Fe(p,p')^{56}Fe^{*}$	8.9×10^{-12}
		$^{56}Fe(\alpha,\alpha')^{56}Fe^{*}$	8.9×10^{-12}
		$^{56}Fe(p,n)^{56}Co(e^{+},\epsilon)^{56}Fe^{*}(100\%)$	9.6×10^{6}
0.891	$^{22}Na^{*0.891} \rightarrow$g.s.	$^{24}Mg(p,x)^{22}Na^{*}$	1.4×10^{-11}
0.931	$^{55}Fe^{*0.931} \rightarrow$g.s.	$^{56}Fe(p,x)^{55}Fe^{*}$	1.2×10^{-11}
		$^{56}Fe(p,x)^{55}Co(e^{+},\epsilon)^{55}Fe^{*}(100\%)$	9.1×10^{4}
0.936	$^{52}Cr^{*2.370} \rightarrow ^{52}Cr^{*1.434}$	$^{56}Fe(p,x)^{52}Mn(e^{+},\epsilon)^{52}Cr^{*}(95\%)$	7.0×10^{5}
0.937	$^{18}F^{*0.937} \rightarrow$g.s.	$^{16}O(^{3}He,p)^{18}F^{\star}$	6.8×10^{-11}

Table 1—Continued

Line[a]	Transition[b]	Reaction	Mean Life[c]
0.957	$^{27}Si^{*0.957} \rightarrow$g.s.	$^{28}Si(p,x)^{27}Si^{*}$	1.7×10^{-12}
0.984	$^{48}Ti^{*0.984} \rightarrow$g.s.	$^{56}Fe(p,x)^{48}Ti^{*}$	6.2×10^{-12}
0.999	$^{59}Ni^{*1.338} \rightarrow ^{59}Ni^{*0.339}$	$^{56}Fe(\alpha,n)^{59}Ni^{*}$	1.4×10^{-12}

[a]Line photon energy in MeV. Data from Firestone & Shirley (1996).

[b]Data from Firestone & Shirley (1996).

[c]Mean life in seconds of the nuclear level or radioactive isotope. Data from Firestone & Shirley (1996). In cases where energy widths were given, we converted these into mean times using the uncertainty principle.

Table 2. Gamma Ray Lines in the Range 1.0-1.45 MeV Ordered by Energy

Line[a]	Transition[b]	Reaction	Mean Life[c]
1.005	$^{58}Ni^{*2.459} \rightarrow ^{58}Ni^{*1.454}$	$^{56}Fe(\alpha,x)^{58}Ni^{*}$	$> 1.4 \times 10^{-12}$
1.014	$^{27}Al^{*1.014} \rightarrow$g.s.	$^{27}Al(p,p')^{27}Al^{*}$	2.1×10^{-12}
		$^{28}Si(p,x)^{27}Al^{*}$	2.1×10^{-12}
1.022	$^{10}B^{*1.740} \rightarrow ^{10}B^{*0.718}$	$^{12}C(p,x)^{10}B^{*}$	7.5×10^{-15}
		$^{16}O(p,x)^{10}B^{*}$	7.5×10^{-15}
1.038	$^{56}Fe^{*3.123} \rightarrow ^{56}Fe^{*2.085}$	$^{56}Fe(p,n)^{56}Co(e^{+},\epsilon)^{56}Fe^{*}(14\%)$	9.6×10^{6}
1.042	$^{18}F^{*1.042} \rightarrow$g.s.	$^{16}O(^{3}He,p)^{18}F^{\star}$	2.6×10^{-15}
1.049	$^{58}Co^{*1.049} \rightarrow$g.s.	$^{56}Fe(\alpha,x)^{58}Co^{*}$	2.2×10^{-13}
1.081	$^{18}F^{*1.081} \rightarrow$g.s.	$^{16}O(^{3}He,p)^{18}F^{\star}$	2.8×10^{-14}
1.130	$^{54}Fe^{*2.538} \rightarrow ^{54}Fe^{*1.408}$	$^{56}Fe(p,x)^{54}Fe^{*}$	5.8×10^{-12}
1.189	$^{59}Ni^{*1.189} \rightarrow$g.s.	$^{56}Fe(\alpha,n)^{59}Ni^{*}$	3.3×10^{-13}
1.190	$^{59}Co^{*1.190} \rightarrow$g.s.	$^{56}Fe(\alpha,p)^{59}Co^{*}$	7.5×10^{-14}
1.223	$^{55}Fe^{*2.539} \rightarrow ^{55}Fe^{*1.317}$	$^{56}Fe(p,x)^{55}Fe^{*}$	1.3×10^{-11}
1.238	$^{56}Fe^{*2.085} \rightarrow ^{56}Fe^{*0.847}$	$^{56}Fe(p,p')^{56}Fe^{*}$	9.2×10^{-13}
		$^{56}Fe(\alpha,\alpha')^{56}Fe^{*}$	9.2×10^{-13}
		$^{56}Fe(p,n)^{56}Co(e^{+},\epsilon)^{56}Fe^{*}(68\%)$	9.6×10^{6}
1.249	$^{31}S^{*1.249} \rightarrow$g.s.	$^{32}S(p,x)^{31}S^{*}$	3.5×10^{-13}
1.266	$^{31}P^{*1.266} \rightarrow$g.s.	$^{32}S(p,x)^{31}P^{*}$	7.5×10^{-13}
		$^{28}Si(\alpha,p)^{31}P^{*}$	7.5×10^{-13}
1.275	$^{22}Ne^{*1.275} \rightarrow$g.s.	$^{22}Ne(p,p')^{22}Ne^{*}$	5.2×10^{-12}
		$^{22}Ne(\alpha,\alpha')^{22}Ne^{*}$	5.2×10^{-12}
1.312	$^{48}Ti^{*2.296} \rightarrow ^{48}Ti^{*0.984}$	$^{56}Fe(p,x)^{48}Ti^{*}$	1.8×10^{-12}
1.317	$^{55}Fe^{*1.317} \rightarrow$g.s.	$^{56}Fe(p,x)^{55}Fe^{*}$	3.0×10^{-12}
1.334	$^{52}Cr^{*2.768} \rightarrow ^{52}Cr^{*1.434}$	$^{56}Fe(p,x)^{52}Cr^{*}$	3.6×10^{-12}
1.367	$^{59}Ni^{*2.705} \rightarrow ^{59}Ni^{*1.338}$	$^{56}Fe(\alpha,n)^{59}Ni^{*}$	5.0×10^{-13}
1.369	$^{24}Mg^{*1.369} \rightarrow$g.s.	$^{24}Mg(p,p')^{24}Mg^{*}$	2.0×10^{-12}
		$^{25}Mg(p,pn)^{24}Mg^{*}$	2.0×10^{-12}
		$^{26}Mg(p,p2n)^{24}Mg^{*}$	2.0×10^{-12}
		$^{24}Mg(\alpha,\alpha')^{24}Mg^{*}$	2.0×10^{-12}
		$^{28}Si(p,x)^{24}Mg^{*}$	2.0×10^{-12}
1.370	$^{55}Fe^{*2.301} \rightarrow ^{55}Fe^{*0.931}$	$^{56}Fe(p,x)^{55}Fe^{*}$	8.7×10^{-13}
1.408	$^{55}Fe^{*1.408} \rightarrow$g.s.	$^{56}Fe(p,x)^{55}Fe^{*}$	5.5×10^{-11}

Table 2—Continued

Line[a]	Transition[b]	Reaction	Mean Life[c]
	$^{54}Fe^{*1.408} \rightarrow$g.s.	$^{56}Fe(p,x)^{54}Fe^{*}$	1.2×10^{-12}
		$^{56}Fe(p,x)^{55}Co(e^{+},\epsilon)^{55}Fe^{*}(23\%)$	9.1×10^{4}
1.428	$^{59}Ni^{*1.767} \rightarrow ^{59}Ni^{*0.339}$	$^{56}Fe(\alpha,n)^{59}Ni^{*}$	8.7×10^{-13}
1.434	$^{52}Cr^{*1.434} \rightarrow$g.s.	$^{56}Fe(p,x)^{52}Cr^{*}$	9.8×10^{-13}
		$^{56}Fe(p,x)^{52}Mn(e^{+},\epsilon)^{52}Cr^{*}(100\%)$	7.0×10^{5}
1.441	$^{53}Mn^{*1.441} \rightarrow$g.s.	$^{56}Fe(p,x)^{53}Mn^{*}$	8.7×10^{-13}

[a]Line photon energy in MeV. Data from Firestone & Shirley (1996).

[b]Data from Firestone & Shirley (1996).

[c]Mean life in seconds of the nuclear level or radioactive isotope. Data from Firestone & Shirley (1996). In cases where energy widths were given, we converted these into mean times using the uncertainty principle.

Table 3. Gamma Ray Lines in the Range 1.45-2.2 MeV Ordered by Energy

Line[a]	Transition[b]	Reaction	Mean Life[c]
1.454	$^{58}Ni^{*1.454} \rightarrow$g.s.	$^{56}Fe(\alpha,x)^{58}Ni^{*}$	9.3×10^{-13}
1.460	$^{59}Co^{*1.460} \rightarrow$g.s.	$^{56}Fe(\alpha,p)^{59}Co^{*}$	1.5×10^{-12}
1.600	$^{23}Mg^{*2.051} \rightarrow ^{23}Mg^{*0.451}$	$^{24}Mg(p,x)^{23}Mg^{*}$	2.9×10^{-14}
1.634	$^{20}Ne^{*1.634} \rightarrow$g.s.	$^{20}Ne(p,p')^{20}Ne^{*}$	1.1×10^{-12}
		$^{20}Ne(\alpha,\alpha')^{20}Ne^{*}$	1.1×10^{-12}
		$^{24}Mg(p,x)^{20}Ne^{*}$	1.1×10^{-12}
		$^{24}Mg(\alpha,x)^{20}Ne^{*}$	1.1×10^{-12}
		$^{28}Si(p,x)^{20}Ne^{*}$	1.1×10^{-12}
1.635	$^{14}N^{*3.948} \rightarrow ^{14}N^{*2.313}$	$^{14}N(p,p')^{14}N^{*}$	6.9×10^{-15}
		$^{14}N(\alpha,\alpha')^{14}N^{*}$	6.9×10^{-15}
		$^{16}O(p,x)^{14}N^{*}$	6.9×10^{-15}
1.636	$^{23}Na^{*2.076} \rightarrow ^{23}Na^{*0.440}$	$^{24}Mg(p,x)^{23}Na^{*}$	3.8×10^{-14}
		$^{24}Mg(\alpha,x)^{23}Na^{*}$	3.8×10^{-14}
1.771	$^{56}Fe^{*3.856} \rightarrow ^{56}Fe^{*2.085}$	$^{56}Fe(p,p')^{56}Fe^{*}$	3.6×10^{-14}
		$^{56}Fe(p,n)^{56}Co(e^{+},\epsilon)^{56}Fe^{*}(16\%)$	9.6×10^{6}
1.779	$^{28}Si^{*1.779} \rightarrow$g.s.	$^{28}Si(p,p')^{28}Si^{*}$	6.9×10^{-13}
		$^{28}Si(\alpha,\alpha')^{28}Si^{*}$	6.9×10^{-13}
		$^{32}S(p,x)^{28}Si^{*}$	6.9×10^{-13}
1.809	$^{26}Mg^{*1.809} \rightarrow$g.s.	$^{26}Mg(p,p')^{26}Mg^{*}$	6.9×10^{-13}
		$^{26}Mg(\alpha,\alpha')^{26}Mg^{*}$	6.9×10^{-13}
		$^{27}Al(p,x)^{26}Mg^{*}$	6.9×10^{-13}
1.811	$^{56}Fe^{*2.658} \rightarrow ^{56}Fe^{*0.847}$	$^{56}Fe(p,p')^{56}Fe^{*}$	3.0×10^{-14}
2.000	$^{11}C^{*2.000} \rightarrow$g.s.	$^{12}C(p,x)^{11}C^{*}$	1.0×10^{-14}
2.029	$^{31}P^{*3.295} \rightarrow ^{31}P^{*1.266}$	$^{32}S(p,x)^{31}P^{*}$	5.5×10^{-14}
2.034	$^{31}S^{*3.283} \rightarrow ^{31}S^{*1.249}$	$^{32}S(p,x)^{31}S^{*}$	$- - -$
2.094	$^{56}Fe^{*.2.942} \rightarrow ^{56}Fe^{*0.847}$	$^{56}Fe(p,p')^{56}Fe^{*}$	6.5×10^{-13}
2.113	$^{56}Fe^{*2.960} \rightarrow ^{56}Fe^{*0.847}$	$^{56}Fe(p,p')^{56}Fe^{*}$	4.0×10^{-14}
2.124	$^{11}B^{*2.125} \rightarrow$g.s.	$^{12}C(p,x)^{11}B^{*}$	5.5×10^{-15}
2.164	$^{27}Si^{2.164} \rightarrow$g.s.	$^{28}Si(p,x)^{27}Si^{*}$	6.3×10^{-14}

[a]Line photon energy in MeV. Data from Firestone & Shirley (1996).

[b]Data from Firestone & Shirley (1996).

[c]Mean life in seconds of the nuclear level or radioactive isotope. Data from Firestone & Shirley (1996). In cases where energy widths were given, we converted these into mean times using the uncertainty principle.

Table 4. Gamma Ray Lines in the Range 2.2-3.5 MeV Ordered by Energy

Line[a]	Transition[b]	Reaction	Mean Life[c]
2.211	$^{27}Al^{*2.211} \rightarrow$g.s.	$^{27}Al(\alpha,\alpha')^{27}Al^*$	3.8×10^{-14}
		$^{24}Mg(\alpha,x)^{27}Al^*$	3.8×10^{-14}
		$^{28}Si(p,x)^{27}Al^*$	3.8×10^{-14}
2.230	$^{32}S^{*2.230} \rightarrow$g.s.	$^{32}S(p,p')^{32}S^*$	1.2×10^{-13}
		$^{32}S(\alpha,\alpha')^{32}S^*$	1.2×10^{-13}
2.232	$^{31}S^{*2.232} \rightarrow$g.s.	$^{32}S(p,x)^{31}S^*$	1.4×10^{-13}
2.234	$^{31}P^{*2.234} \rightarrow$g.s.	$^{32}S(p,x)^{31}P^*$	3.6×10^{-13}
		$^{28}Si(\alpha,p)^{31}P^*$	3.6×10^{-13}
2.235	$^{30}Si^{*2.235} \rightarrow$g.s.	$^{27}Al(\alpha,x)^{30}Si^*$	3.6×10^{-13}
2.263	$^{23}Na^{*2.704} \rightarrow ^{23}Na^{*0.440}$	$^{20}Ne(\alpha,x)^{23}Na^*$	1.1×10^{-13}
2.313	$^{14}N^{*2.313} \rightarrow$g.s.	$^{14}N(p,p')^{14}N^*$	9.8×10^{-14}
		$^{14}N(\alpha,\alpha')^{14}N^*$	9.8×10^{-14}
		$^{14}N(p,n)^{14}O(e^+,\epsilon)^{14}N^{*2.313}$	102
		$^{16}O(p,x)^{14}N^*$	9.8×10^{-14}
2.598	$^{56}Fe^{*3.449} \rightarrow ^{56}Fe^{*0.847}$	$^{56}Fe(p,n)^{56}Co(e^+,\epsilon)^{56}Fe^*(17\%)$	9.6×10^{6}
2.614	$^{20}Ne^{*4.248} \rightarrow ^{20}Ne^{*1.634}$	$^{20}Ne(p,p')^{20}Ne^*$	9.2×10^{-14}
		$^{20}Ne(\alpha,\alpha')^{20}Ne^*$	9.2×10^{-14}
		$^{24}Mg(p,x)^{20}Ne^*$	9.2×10^{-14}
		$^{28}Si(p,x)^{20}Ne^*$	9.2×10^{-14}
2.640	$^{23}Na^{*2.640} \rightarrow$g.s.	$^{24}Mg(p,x)^{23}Na^*$	9.7×10^{-14}
2.742	$^{16}O^{*8.872} \rightarrow ^{16}O^{*6.130}$	$^{16}O(p,p')^{16}O^*$	1.8×10^{-13}
		$^{16}O(\alpha,\alpha')^{16}O^*$	1.8×10^{-13}
2.754	$^{24}Mg^{*4.123} \rightarrow ^{24}Mg^{*1.369}$	$^{24}Mg(p,p')^{24}Mg^*$	3.5×10^{-14}
		$^{25}Mg(p,pn)^{24}Mg^*$	3.5×10^{-14}
		$^{26}Mg(p,p2n)^{24}Mg^*$	3.5×10^{-14}
		$^{24}Mg(\alpha,\alpha')^{24}Mg^*$	3.5×10^{-14}
3.333	$^{20}Ne^{*4.967} \rightarrow ^{20}Ne^{*1.634}$	$^{20}Ne(p,p')^{20}Ne^*$	4.8×10^{-12}
		$^{20}Ne(\alpha,\alpha')^{20}Ne^*$	4.8×10^{-12}

[a]Line photon energy in MeV. Data from Firestone & Shirley (1996).

[b]Data from Firestone & Shirley (1996).

[c]Mean life in seconds of the nuclear level or radioactive isotope. Data from Firestone & Shirley (1996). In cases where energy widths were given, we converted these into mean times using the uncertainty principle.

Table 5. Gamma Ray Lines in the Range 3.5-5.2 MeV Ordered by Energy

Line[a]	Transition[b]	Reaction	Mean Life[c]
3.562	$^{6}Li^{*3.563} \rightarrow$g.s.	$^{4}He(\alpha,pn)^{6}Li^{*}$	1.2×10^{-16}
		$^{4}He(^{3}He,p)^{6}Li^{*}$	1.2×10^{-16}
3.684	$^{13}C^{*3.685} \rightarrow$g.s.	$^{13}C(p,p')^{13}C^{*}$	1.6×10^{-15}
		$^{13}C(\alpha,\alpha')^{13}C^{*}$	1.6×10^{-15}
		$^{16}O(p,x)^{13}C^{*}$	1.6×10^{-15}
3.736	$^{40}Ca^{*3.736} \rightarrow$g.s.	$^{40}Ca(p,p')^{40}Ca^{*}$	2.9×10^{-11}
		$^{40}Ca(\alpha,\alpha')^{40}Ca^{*}$	2.9×10^{-11}
3.853	$^{13}C^{*3.854} \rightarrow$g.s.	$^{13}C(p,p')^{13}C^{*}$	1.2×10^{-11}
		$^{13}C(\alpha,\alpha')^{13}C^{*}$	1.2×10^{-11}
		$^{16}O(p,x)^{13}C^{*}$	1.2×10^{-11}
4.438	$^{12}C^{*4.439} \rightarrow$g.s.	$^{12}C(p,p')^{12}C^{*}$	6.1×10^{-14}
		$^{12}C(\alpha,\alpha')^{12}C^{*}$	6.1×10^{-14}
		$^{14}N(p,x)^{12}C^{*}$	6.1×10^{-14}
		$^{14}N(\alpha,x)^{12}C^{*}$	6.1×10^{-14}
		$^{16}O(p,x)^{12}C^{*}$	6.1×10^{-14}
		$^{16}O(\alpha,x)^{12}C^{*}$	6.1×10^{-14}
4.444	$^{11}B^{*4.445} \rightarrow$g.s.	$^{12}C(p,2p)^{11}B^{*}$	5.6×10^{-19}
		$^{12}C(\alpha,x)^{11}B^{*}$	5.6×10^{-19}
		$^{14}N(p,x)^{11}B^{*}$	5.6×10^{-19}
5.099	$^{28}Si^{*6.879} \rightarrow ^{28}Si^{*1.779}$	$^{28}Si(p,p')^{28}Si$	1.2×10^{-12}
		$^{28}Si(\alpha,\alpha')^{28}Si$	1.2×10^{-12}
5.105	$^{14}N^{*5.106} \rightarrow$g.s.	$^{14}N(p,p')^{14}N^{*}$	6.3×10^{-12}
		$^{14}N(\alpha,\alpha')^{14}N^{*}$	6.3×10^{-12}
		$^{16}O(p,x)^{14}N^{*}$	6.3×10^{-12}
		$^{16}O(\alpha,x)^{14}N^{*}$	6.3×10^{-12}
5.180	$^{15}O^{5.181} \rightarrow$g.s.	$^{16}O(p,x)^{15}O^{*}$	$< 4.9 \times 10^{-14}$
		$^{16}O(\alpha,x)^{15}O^{*}$	$< 4.9 \times 10^{-14}$

[a]Line photon energy in MeV. Data from Firestone & Shirley (1996).

[b]Data from Firestone & Shirley (1996).

[c]Mean life in seconds of the nuclear level or radioactive isotope. Data from Firestone & Shirley (1996). In cases where energy widths were given, we converted these into mean times using the uncertainty principle.

Table 6. Gamma Ray Lines Above 5.2 MeV Ordered by Energy

Line[a]	Transition[b]	Reaction	Mean Life[c]
5.240	$^{15}O^{*5.241} \rightarrow$g.s.	$^{12}C(\alpha,x)^{15}O^*$	3.25×10^{-12}
		$^{16}O(p,x)^{15}O^*$	3.25×10^{-12}
		$^{16}O(\alpha,x)^{15}O^*$	3.25×10^{-12}
5.269	$^{15}N^{*5.270} \rightarrow$g.s.	$^{12}C(\alpha,x)^{15}N^*$	2.58×10^{-12}
		$^{16}O(p,x)^{15}N^*$	2.58×10^{-12}
		$^{16}O(\alpha,x)^{15}N^*$	2.58×10^{-12}
5.298	$^{15}N^{*5.299} \rightarrow$.g.s.	$^{16}O(p,x)^{15}N^*$	1.2×10^{-14}
		$^{16}O(\alpha,x)^{15}N^*$	1.2×10^{-14}
6.129	$^{16}O^{*6.130} \rightarrow$g.s.	$^{16}O(p,p')^{16}O^*$	2.7×10^{-11}
		$^{16}O(\alpha,\alpha')^{16}O^*$	2.7×10^{-11}
		$^{20}Ne(p,x)^{16}O^*$	2.7×10^{-11}
6.175	$^{15}O^{*6.176} \rightarrow$g.s.	$^{16}O(p,x)^{15}O^*$	$< 2.3 \times 10^{-14}$
6.322	$^{15}N^{*6.324} \rightarrow$g.s.	$^{16}O(p,x)^{15}N^*$	1.0×10^{-15}
6.337	$^{11}C^{*6.339} \rightarrow$g.s.	$^{12}C(p,x)^{11}C^*$	$< 1.1 \times 10^{-13}$
		$^{12}C(\alpha,x)^{11}C^*$	$< 1.1 \times 10^{-13}$
6.476	$^{11}C^{*6.478} \rightarrow$g.s.	$^{12}C(p,x)^{11}C^*$	$< 8.7 \times 10^{-15}$
		$^{12}C(\alpha,x)^{11}C^*$	$< 8.7 \times 10^{-15}$
6.741	$^{11}B^{*6.743} \rightarrow$g.s.	$^{12}C(p,x)^{11}B^*$	4.3×10^{-20}
		$^{12}C(\alpha,x)^{11}B^*$	4.3×10^{-20}
6.790	$^{11}B^{*6.792} \rightarrow$g.s.	$^{12}C(p,x)^{11}B^*$	5.6×10^{-19}
		$^{12}C(\alpha,x)^{11}B^*$	5.6×10^{-19}
6.879	$^{28}Si^{*6.879} \rightarrow$g.s.	$^{28}Si(p,p')^{28}Si^*$	1.2×10^{-12}
		$^{28}Si(\alpha,\alpha')^{28}Si^*$	1.2×10^{-12}
6.916	$^{16}O^{*6.917} \rightarrow$g.s.	$^{16}O(p,p')^{16}O^*$	6.8×10^{-15}
		$^{16}O(\alpha,\alpha')^{16}O^*$	6.8×10^{-15}
7.115	$^{16}O^{*7.117} \rightarrow$g.s.	$^{16}O(p,p')^{16}O^*$	1.2×10^{-14}
		$^{16}O(\alpha,\alpha')^{16}O^*$	1.2×10^{-14}
7.299	$^{15}N^{*7.301} \rightarrow$g.s.	$^{16}O(p,x)^{15}N^*$	1.4×10^{-16}
		$^{16}O(\alpha,x)^{15}N^*$	1.4×10^{-16}
15.10	$^{12}C^{*15.11} \rightarrow$g.s.	$^{12}C(p,p')^{12}C^*$	1.5×10^{-17}

[a]Line photon energy in MeV. Data from Firestone & Shirley (1996).

[b]Data from Firestone & Shirley (1996).

[c]Mean life in seconds of the nuclear level or radioactive isotope. Data from Firestone & Shirley (1996). In cases where energy widths were given, we converted these into mean times using the uncertainty principle.